LUND UNIVERSITY

Dysfunctional but viable myocardium - ischemic heart disease assessed by magnetic resonance imaging and single photon emission computed tomography

Ugander, Martin

2005

Total number of authors:
1

Dysfunctional but viable myocardium

Ischemic heart disease assessed by magnetic resonance imaging and single photon emission computed tomography

MARTIN UGANDER, M.D.

LUND UNIVERSITY

Doctoral Thesis
2005

Department of Clinical Physiology
Lund University, Sweden

Faculty opponent
Professor Robert O. Bonow, M.D., Division of Cardiology,
Northwestern University, Chicago, IL, USA

Cover:
Magnetic resonance images of the heart of a patient with ischemic heart disease and dysfunctional but viable myocardium. The left image was taken before contrast injection and shows the end systolic time frame from a series of time-resolved images. The left ventricular ejection fraction was 25%. The right image was take in the same slice position after contrast injection and shows viable myocardium as black and infarcted myocardium as white. The infarct size was 6% of the total left ventricular myocardium. For details see appended Paper III, Figure 5.

The road to wisdom - well, it's plain
and simple to express:
  Err
  and err
  and err again,
  but less,
  and less,
  and less.

      —PIET HEIN

Contents

List of Papers

This thesis is based on the following papers, which will be referred to by their Roman numerals in the text.

I. Cain PA, **Ugander M**, Palmer J, Carlsson M, Heiberg E, Arheden H. Quantitative polar representation of left ventricular myocardial perfusion, function and viability using SPECT and cardiac magnetic resonance: initial results. *Clin Physiol Funct Imaging.* 2005;25:215-222.

II. **Ugander M**, Cain PA, Perron A, Hedstrom E, Arheden H. Infarct transmurality and adjacent segmental function as determinants of wall thickening in revascularized chronic ischemic heart disease. *Clin Physiol Funct Imaging.* 2005;25:209-214.

III. **Ugander M**, Ekmehag B, Arheden H. A maximum predicted left ventricular ejection fraction in relation to infarct size in patients with ischemic heart disease. *Submitted.*

IV. **Ugander M**, Cain P, Johnsson P, Palmer J, Arheden H. Influence of the presence of chronic non-transmural myocardial infarction on the time course of perfusion and functional recovery after revascularization. *Manuscript.*

Summary

The assessment of ischemic heart disease (IHD) often focuses on the detection of dysfunctional but viable myocardium which may improve in function following revascularization. Dysfunctional but viable myocardium is identified by distinct characteristics with regards to function, perfusion and viability. Therefore, in Paper I we developed a method for quantitative polar representation of left ventricular myocardial function, perfusion and viability using single photon emission computed tomography (SPECT) and cardiac magnetic resonance (CMR). Polar representation of these parameters was feasible, and the quantitative method agreed with visual assessment.

Paper II showed that wall thickening decreases with increasing infarct transmurality. However, the variation in wall thickening was large, and importantly, influenced more so by the function of adjacent myocardium than by infarct transmurality. This underscores the difficulty of using resting function alone to accurately assess myocardial infarction in revascularized IHD.

In Paper III we assessed the relationship between left ventricular ejection fraction (LVEF) and infarct size and found that LVEF cannot be used to estimate infarct size, and vice versa. However, the study showed that LVEF can be used to estimate a maximum predicted infarct size, and that infarct size can be used to estimate a maximum predicted LVEF. These results emphasize the importance of direct infarct imaging by CMR when attempting to estimate the size of infarction in patients with IHD.

Paper IV was designed to assess the time course of recovery of myocardial perfusion and function after revascularization. The recovery of perfusion was found to occur in the first month, while the recovery of function was delayed in segments with non-transmural infarction.

In summary, the presented studies emphasize the importance of direct infarct imaging by CMR for the accurate identification of infarction in the assessment of dysfunctional myocardium. Neither regional nor global myocardial function have a close correlation to infarction, but the presence of non-transmural infarction is a marker for delayed recovery of function following revascularization.

Populärvetenskaplig sammanfattning

En hjärtinfarkt definieras som celldöd i hjärtmuskeln, och om celldöden är omfattande, orsakar den en oåterkallelig nedsättning i hjärtats pumpfunktion. Pumpfunktionen kan även vara långvarigt nedsatt p.g.a. att hjärtat inte får tillräckligt med blod. Man kan då förbättra pumpfunktionen genom att återställa blodtillförseln med en operation. För att kunna hitta områden i hjärtat med nedsatt funktion men levande hjärtmuskel ("dysfunctional but viable myocardium") är det nödvändigt att bedöma tre egenskaper: (1) hjärtats pumpfunktion, (2) dess genomblödning (perfusion) och (3) huruvida cellerna lever eller ej.

Delarbete I beskriver utvecklingen av en ny metod för att objektivt mäta dessa tre egenskaper med hjälp av funktionsbilder och infarktbilder från magnetisk resonanstomografi (MR) och bilder av perfusion från SPECT (en metod för att avbilda hjärtmuskelns genomblödning med en radioaktiv isotop som injiceras i blodet). Metoden implementerades och mätresultaten visade god överensstämmelse med visuell bedömning.

Delarbete II visar att pumpfunktionen i ett område beror mer på funktionen i omgivande hjärtmuskel än på utbredningen av infarkt i området. Delarbete III visar att hjärtats totala pumpfunktion varierar påtagligt i förhållande till den totala infarktstorleken, men att det föreligger en maximalt förväntad pumpfunktion i förhållande till infarktstorlek. Dessa arbeten visar att det varken går att påvisa eller utesluta förekomsten av infarkt genom att endast värdera pumpfunktionen.

Delarbete IV visar att även om perfusionen ökar tidigt efter en operation så kan funktionsåterhämtningen i levande hjärtmuskel vara fördröjd i områden i nära anslutning till infarkt. Detta ökar vår förståelse för återhämtningsförloppet efter en operation.

Varken regional eller total pumpfunktion korrelerar starkt till infarkt, men områden som delvis drabbats av infarkt uppvisar fördröjd funktionsåterhämtning efter operation. Sammanfattningsvis visar avhandlingen på vikten av att direkt avbilda infarkt med MR för att kunna bedöma möjligheten till funktionsåterhämtning i hjärtmuskel efter operation.

Abbreviations

ATP	adenosine triphosphate
Ao	aortic valve
CABG	coronary artery bypass grafting
CAD	coronary artery disease
CIHD	chronic ischemic heart disease
CT	computed tomography
CM	non-ischemic cardiomyopathy
CMR	cardiac magnetic resonance
CO	cardiac output (l/min)
DE	delayed contrast enhanced
DTPA	diethylenetriamine penta-acetic acid
EBCT	electron beam computed tomography
ECG	electrocardiogram
ED	end diastole
EDV	end diastolic volume (ml)
EF	ejection fraction (%)
ES	end systole
ESV	end systolic volume (ml)
^{18}F	fluorine
^{18}FDG	fluorodeoxyglucose
FV	forward volume
Gd	gadolinium
HR	heart rate (beats/min)
HU	Hounsfield units
IHD	ischemic heart disease
IS	infarct size
IVUS	intravascular ultrasound
LV	left ventricle
LVM	left ventricular myocardium (ml)

MCE	myocardial contrast echocardiography
MIBI	2-methoxy-isobutyl-isonitrile
$_{mitral}$	mitral valve
MLEM	maximum likelihood-expectation maximization
MPS	myocardial perfusion SPECT
MRI	magnetic resonance imaging
NVM	non-viable myocardium
PC	phase contrast
PCI	percutaneous coronary intervention
PET	positron emission tomography
RF	regurgitant fraction
RF	radio frequency
ROI	region of interest
RV	regurgitant volume
SD	standard deviation
SEM	standard error of the mean
SNR	signal-to-noise ratio
SPECT	single photon emission computed tomography
SSFP	steady state free precession
SV	stroke volume (ml)
T	Tesla
^{99m}Tc	technetium
^{201}Tl	thallium
VCG	vectorcardiography
W	Kendall's coefficient of concordance

Chapter 1

Introduction

1.1 Ischemic heart disease

Ischemic heart disease (IHD) is the primary cause of left ventricular dysfunction leading to heart failure in Europe.[1] The number of patients who develop heart failure has been increasing exponentially. In the United States, it was recently estimated that 550,000 new cases of chronic heart failure are identified each year, yielding 970,000 hospitalizations per year and a total of 4.9 million patients.[2] Furthermore, it is estimated that 70% of heart failure can be attributed to coronary artery disease (CAD).[3] Taken together, IHD is the leading cause of morbidity and mortality in the Western world,[4] and it is rapidly increasing in developing countries.[5]

1.1.1 Pathophysiology

The ischemic cascade

An understanding of ischemic heart disease (IHD) involves an understanding of the sequence of pathophysiological events that occur during ischemia. This temporal sequence of events is illustrated in Figure 1.1 and is called *the ischemic cascade*.[6]

Ischemia is defined as an imbalance between myocardial oxygen supply and demand. If myocardium is affected by severe enough ischemia for a sufficient duration of time then the ultimate consequence is irreversible cell death. This is represented by infarction, seen at the right extreme of the ischemic cascade. However, before infarction develops, there are several physiological states of myocardial dysfunction which can be reversed if the ischemia is alleviated.

The term *non-viable myocardium* will hereby be used to describe myocard-
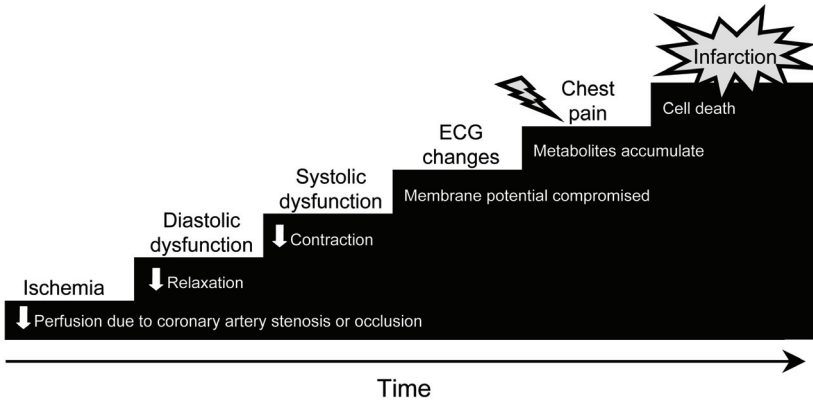
FIGURE 1.1 The ischemic cascade, illustrating the sequence of pathophysiological events in relation to the duration of ischemia.

ium which has been irreversibly damaged by infarction. The terms *viability* and *viable myocardium* have been used extensively in the literature to selectively describe reversibly dysfunctional myocardium while excluding normally functioning myocardium which also is alive.[7] However, the term *viable* will herein be used to describe all myocardium − normal and dysfunctional − which is not irreversibly damaged.[8] The term *dysfunctional but viable myocardium* will instead be used to selectively describe myocardium with intact cell membranes and which is in a state of potentially reversible dysfunction. Dysfunction in this setting refers to reduced systolic function at rest. Thus, the ischemic cascade describes the different pathophysiological events which occur during ischemia and the evolution of dysfunctional but viable myocardium, and ultimately infarction.

The first event in the ischemic cascade is a reduction in perfusion. Reduced perfusion may be caused either by progressive stenosis due to the development of atherosclerotic plaque, or acute occlusion due to thrombosis at the site of a plaque rupture.[9]

If the reduction in perfusion is severe enough to cause ischemia, this initially results in impaired myocardial relaxation, otherwise known as *diastolic dysfunction*. Relaxation is the energy-dependent phase of the contractile cycle in the cardiac myocyte, and it is limited by the supply of energy from adenosine triphosphate (ATP). ATP is necessary during relaxation in order to pump Ca^{++} from the cytosol back into the sarcoplasmatic reticulum through ATP-dependent Ca^{++} channels.[10] Hence, when ischemia reduces the supply of ATP, then relaxation is the first process to be influenced.

Furthermore, as ischemia persists, reduced amounts of creatine phosphate[11] and the free energy hydrolysis of ATP[12] both contribute to the continued reduction in the amount of ATP. Thus, the accumulated ATP debt further impacts on the ATP-dependent transport of Ca^{++} and contraction is impaired. *Systolic dysfunction* is the result of this compromised contraction in addition to compromised relaxation.

Further ATP debt effects the ATP-dependent Na^+/K^+ pump in the cell membrane.[13] Disturbances in depolarization, repolarization and ultimately failure to sustain the membrane potential can be observed as changes in the electrocardiogram (ECG).

The accumulation of metabolites eventually leads to the development of *chest pain*, possibly due to the accumulation of adenosine.[14] Finally, if ischemia persists long enough, the result is irreversible cell rupture and necrosis which starts at the endocardium and progresses as a wavefront of necrosis — *infarction* — towards the epicardium.[15]

In summary, the ischemic cascade describes a sequence of physiological observations which are involved in the development of dysfunctional but viable myocardium. However, subtypes of dysfunctional but viable myocardium can readily be identified based on unique combinations of physiological characteristics and their appropriate treatment. Notably, accurate classification by necessity includes assessment of both perfusion, function and viability. It is not possible to accurately classify dysfunctional but viable myocardium from a pathophysiological perspective if any one of these three physiological characteristics is left out of an assessment.

Dysfunctional but viable myocardium

Dysfunctional but viable myocardium can be categorized into subtypes based on important differences with regards to presence or absence of compromised perfusion, function, cellular integrity and need for revascularization. The characteristics of different categories of ischemically compromised myocardium are summarized in Table 1.1.

Stress induced ischemia. Stress induced ischemia is characterized by viable myocardium which has normal perfusion and function at rest, but where perfusion and function are compromised at stress. Stress represents an increased oxygen demand which typically can be achieved by for example physical exertion, increased sympathetic discharge leading to increased heart rate, increased blood pressure and increased wall tension.[17] Stress can also be induced pharmacologically. Patients exhibiting stress induced ischemia will benefit from revascularization, particularly those with a large extent of stress induced ischemia.[18]

One should be aware that this definition of stress induced ischemia represents

TABLE 1.1
Physiological characteristics used to define different categories of
ischemically compromised myocardium.

| | Function | | Perfusion | | Cell | Need for |
	rest	stress	rest	stress	death	revasc.
Normal	norm	norm	norm	norm	no	no
Stress induced ischemia	norm	↓	norm	↓	no	yes
Stunning	↓	↓	norm	norm	no	no
Repetitive stunning	↓	↓	norm	↓	no*	yes
Hibernation	↓	↓	↓	↓	no*	yes
Infarction	↓	↓	↓	↓	yes	no

* Repetitive stunning or hibernation may induce cellular morphological changes which are characterized by both adaptive and degenerative features,[16] but not widespread necrosis as is seen in myocardial infarction. norm = normal, revasc. = revascularization

a simplified definition which is presented for purposes of comparison. It should be acknowledged that situations may occur where the duration of stress induced ischemia is short enough to only induce a reduction in perfusion, but not sufficient enough to induce a reduction in systolic function. Likewise, situations may occur where the duration of ischemia due to stress may be sufficient to induce a prolonged but ultimately reversible reduction in function. This case of prolonged resting dysfunction will now be discussed.

Stunned myocardium. Stunned myocardium is characterized by a prolonged postischemic reduction in function in the presence of normal perfusion and the absence of infarction.[19] The classic definition of stunning stems from observations of a prolonged but reversible reduction in systolic function following successful restoration of perfusion in the setting of experimental occlusion and reperfusion,[20] and later, acute occlusion and reperfusion in the clinical setting of ST-

elevation myocardial infarction.[21, 22] In these settings, rest and stress perfusion will both have been restored to normal and the observed reduction in function will spontaneously resolve with time. Therefore, it is not necessary *per se* to revascularize stunned myocardium according to this classical definition.

There are, however, situations where stunning occurs as a result of stress induced ischemia and would thereby require revascularization. Such scenarios will be discussed shortly.

The cellular mechanisms governing stunning have not been completely elucidated. Dominant views include the influence of oxidant stress from reactive oxygen species, as well as disturbances in calcium homeostasis.[23, 24]

Repetitive stunning. Reduced function at rest is an important part of the definition of dysfunctional but viable myocardium, including stunning. As discussed above, stress induced ischemia of sufficient severity and duration may induce a reduction in function which persists despite the return of normal resting perfusion. This has been observed in both experimental animals[25] and patients with effort angina.[26] These patients have stress induced ischemia and if they are not revascularized, the risk of stunning is repeatedly present whenever these patients are subjected to sufficient stress. Furthermore, such repetitive stunning cumulatively induces a greater reduction in postischemic resting function than one episode alone.[27, 28] In summary, myocardium exhibiting repetitive stunning is repeatedly stunned by stress induced ischemia and should therefore be revascularized.

Hibernating myocardium. Hibernating myocardium is defined as "a state of persistently impaired myocardial and left ventricular function at rest due to reduced coronary blood flow that can be partially or completely restored to normal if the myocardial oxygen supply/demand relationship is favorably altered, either by improving blood flow and/or by reducing demand."[29] Thus, hibernating myocardium is characterized by a chronic reduction in resting function as an adaptation to reduced resting perfusion in the absence of infarction. Clinical studies have shown that myocardium with reduced function and perfusion at rest may regain function following improvement in resting perfusion by revascularization.[30–35]

The ultrastructural and histological morphology of hibernating myocardium has been studied using transmural needle biopsies taken at the time of open heart surgery. In summary, the features include signs of atrophy, most notably in the contractile myofibrils and signs of degeneration and possibly dedifferentiation, most notably in the interstitial space.[16] The severity of interstitial fibrosis has been shown to increase with increased duration of the clinical ischemia.[36] Also, the amount of myocytes with excess glycogen is exponentially related to the time required for functional recovery following revascularization.[37] Importantly though, non-invasive assessment of changes in perfusion and metabolism cannot distinguish between myocardium of mild or severe histological degeneration.[38]

Controversy exists regarding whether hibernating myocardium with reduced

resting function and perfusion readily exists, or if the more common mechanism for resting dysfunction is normal resting perfusion which is repeatedly stunned due to a reduced coronary flow reserve.[16]

An experimental model of hibernation in swine sustained for one month has shown normal resting perfusion in 34% of dysfunctional but viable myocardium.[39] However, studies of patients with chronic IHD have shown normal resting perfusion in approximately 90% of dysfunctional but viable myocardium.[40,41] These clinical data support the notion that dysfunctional but viable myocardium is predominantly comprised of repetitive stunning. By comparison, a review of 26 studies comprising 372 patients undergoing quantitative assessment of resting myocardial blood flow in dysfunctional but viable myocardium showed that 49% of the patients were found to have significantly reduced resting perfusion in dysfunctional but viable myocardium compared to normal myocardium.[16] Furthermore, others have identified hibernating myocardium in >20% of the left ventricle (LV) in as many as 30-40% of patients with IHD and an LV ejection fraction (EF) $\leq$30%.[42,43] It is possible that these differences in findings regarding the prevalence of hibernating myocardium reflect differences in patient selection criteria in these reports.

Also, the findings of serially assessed improvement in resting perfusion and function following revascularization[30–35] support the notion that dysfunctional but viable myocardium with reduced resting perfusion does exist. These data favor the concept that hibernating myocardium with some degree of reduced resting perfusion is a considerable component of dysfunctional but viable myocardium.

Importantly for the clinician, dysfunctional but viable myocardium due to either repetitive stunning or hibernating myocardium both show reduced perfusion at *stress*. Reduced resting perfusion appears to be less prevalent in dysfunctional but viable myocardium but can nonetheless exist. Furthermore, it is likely that both hibernation and repetitive stunning may coexist in the same patient and even the same region of myocardium.[44] This implies a downregulation in function as an adaptation to reduced resting perfusion, but also an exacerbation of the compromise in function and perfusion at stress. Hence, the exact differentiation between hibernation and repetitive stunning may be of lesser clinical importance. The identification of dysfunctional but viable myocardium in need of revascularization — regardless of subtype — is of paramount importance.[45]

1.1.2 Treatment

Dysfunctional but viable myocardium in the form of both repetitive stunning and hibernating myocardium is characterized by a reduced coronary flow reserve. This coronary flow reserve can be treated by medication and/or surgical[46] or percutaneous[47] revascularization.

Medical treatment includes the use of angiotensin converting enzyme inhibitors,[48] β-blockers,[49] angiotensin II inhibitors[50] and/or amiodarone.[51] Despite advances in medication, however, heart failure has been shown to have a considerable 1 year mortality of 38% and 5 year mortality of >70%.[52]

Surgical revascularization has previously been associated with high periprocedural morbidity and mortality.[53] However, surgery has nonetheless proven to result in improved survival compared to medical treatment.[54]

1.2   Cardiac imaging techniques

There are a number of techniques which make it possible to generate images of the heart without having to open the chest. These cardiac imaging techniques vary considerably with regards to the basic principles governing how the images are generated. Importantly, these principles dictate the particular advantages and limitations of the technique with regards to the assessment of cardiac anatomy and physiology.

This section on cardiac imaging techniques focuses on giving a general overview of the principles governing the most commonly used imaging modalities in cardiac imaging with a particular focus on magnetic resonance imaging (MRI) and single photon emission computed tomography (SPECT). A summary of selected properties of the respective cardiac imaging techniques is presented in Table 1.2.

1.2.1   Echocardiography

Images from the reflection of ultrasound

Echocardiography is a technique that generates images of the heart based on the transmission, reflection and detection of inaudible high frequency sound in human tissue.[55] Echocardiography was discovered in 1953 by the cardiologist Inge Edler and physicist Hellmuth Hertz from Lund University and for which they were awarded the Lasker Award in 1977.

The reflection of ultrasound in human tissue is determined by what is called *acoustic impedance* which is a product of the velocity of sound in the tissue and the density of the tissue. Boundaries between tissues that differ in acoustic impedance, such as the blood and myocardium, generate echoes that are visible as contours in the resulting image.

Doppler principle

In addition to generating anatomical images, echocardiography also makes use of the *Doppler principle* to measure velocities. The Doppler principle states that the

TABLE 1.2
Properties of different cardiac imaging techniques

	Basic principle	Ionizing radiation	Spatial resolution (mm) *	Temporal resolution (ms) *
Echo	reflected sound	no	1×2×2	20
X-ray	external energy transmission	yes	0.25×0.25	6
CT	external energy transmission	yes	0.6×0.6×0.6	170
SPECT	energy emission from injected tracer	yes	10×10×10	70
PET	energy emission from injected tracer	yes	5×5×5	70
MRI	external stimulation of tissue which then emits energy	no	1.2×1.2×8	30

* Values represent typical parameters for clinical assessment of cardiac function, anatomy or perfusion using state-of-the art equipment. See text for details regarding the respective techniques.

reflection of sound from a moving object results in a shift in frequency of that sound. This frequency shift is proportional to the velocity of the moving object. In echocardiography, the Doppler principle can be used to measure the velocity of either the blood or myocardial tissue.

Transducer

Echocardiographic images are generated by applying a *transducer* directly to the area of interest. The transducer acts as a simultaneous ultrasound transmitter and detector. Images of anatomy and/or Doppler derived velocities can be imaged in real-time in one, two or three spatial dimensions over time.

Contrast echocardiography

Inert gas-filled *microbubbles* can be administered by intravenous infusion in order to manipulate the acoustic impedance of the blood and myocardium.[56] Microbubbles can be used to improve visualization of the blood pool or to visualize ischemia-induced changes in blood flow in the myocardium.

Resolution

The *spatial resolution* in ultrasound is different in different directions. In 2D imaging, the transducer transmits and detects ultrasound linearly along scan lines that are distributed like a fan beam. The spatial resolution along the scan lines — the axial resolution — is limited by the depth of the ultrasound pulses. This depth varies with the frequency used. The axial resolution in transthoracic echocardiography is typically 1 mm or less when using frequencies around 5 MHz. The spatial resolution between the scan lines — the lateral resolution — depends on the shape of the fan beam, the ultrasound frequency and the depth. The lateral resolution in echocardiography at the depth of the heart is typically a few millimeters. The slice thickness varies similarly to the lateral resolution and is also typically a few millimeters at the depth of the heart.

The speed with which images can be acquired — the *temporal resolution* — is an important parameter in cardiac imaging since it has implications for the detection of rapid physiological events. Real-time 2D echocardiography is theoretically limited by the speed of sound and can readily achieve a temporal resolution of one image every 3 ms. For purposes of data storage and physiological relevance, clinical imaging is typically undertaken at one image every 10-30 ms.

Technical strengths and limitations

The strengths of the echocardiographic technique include safety, cost, widespread availability and bedside portability. The spatial resolution is very good and the temporal resolution is excellent.

However, it is impossible to acquire images of sufficient quality in up to 25% of patients. This is due to anatomy and acoustic properties. Ultrasound is not transmitted adequately through either air in the lungs or bone. Finally, the position of the echocardiographic imaging plane is maintained manually and this can introduce errors when attempting to image a structure repeatedly over time.

1.2.2   X-ray fluoroscopy

Real-time X-ray movies

X-ray fluoroscopy is the use of X-rays to image the human body in real time. The most common application of X-ray fluoroscopy in cardiac imaging is *coronary angiography*. X-rays and their potential for medical imaging were discovered by the German physicist Wilhelm Conrad Röntgen in 1895. Röntgen was awarded the 1901 Nobel Prize in Physics for his discovery. An X-ray is a form of ionizing electromagnetic radiation. Sufficient X-ray exposure can cause radiation burning of the skin or the induction of cancer through damaging effects on human DNA.

An X-ray fluoroscope is composed of a source of X-ray transmission and a detector. Images are generated based on the contrast between x-rays that reach the detector and those that are absorbed or scattered − *attenuated* − by dense tissues such as bone.

Coronary angiography

Coronary angiography using X-ray fluoroscopy is an invasive procedure. An iodinated contrast medium which attenuates X-rays is injected into the blood. Coronary angiography is the reference standard for assessment of *stenosis* or narrowing of interior the coronary arteries.

At the time of coronary angiography, it is also possible to perform additional invasive assessment of the coronary arteries. Different catheters with either a miniaturized ultrasound transducer tip, a pressure sensitive tip or a Doppler flow wire can be threaded into the coronary arteries. Intravascular ultrasound (IVUS) can provide valuable information regarding thickening of the arterial wall which otherwise cannot be appreciated by assessment of the coronary lumen alone. Changes in flow or pressure over a stenosis can be assessed at both rest and pharmacologically induced hyperemia. Importantly, if a flow limiting stenosis is identified at coronary angiography, revascularization by implantation of a *stent* using balloon angioplasty can be performed, otherwise known as *percutaneous coronary intervention* (PCI).

Resolution

The spatial resolution of invasive coronary angiography depends on the distance between the X-ray source, the object being imaged, and the detector. In clinical application the spatial resolution is typically 0.25x0.25 mm. X-ray fluoroscopic images are projection images and therefore, they have no slice thickness in the traditional sense of the term. It takes 6 ms to acquire an image using x-ray flu-

oroscopy. However, for purposes of reducing radiation exposure, coronary angiography is typically performed with the acquisition of one image every 80 ms.

Technical strengths and limitations

X-ray fluoroscopic invasive coronary angiography has unsurpassed image contrast combined with excellent spatial and temporal resolution. Because it is invasive it offers unique additional possibilities for invasive assessment of stenotic flow and pressure as well as vessel wall imaging.

However, invasive coronary angiography involves the use of ionizing radiation, is a very costly procedure and has a mortality rate of approximately 1 in 1000 procedures.[57] Notably, the contrast medium can cause complications such as life threatening acute allergic reactions or kidney damage, particularly in patients with pre-existing reduced kidney function. Importantly, X-ray fluoroscopy as such is a two dimensional projection imaging technique which can only image the arterial lumen.

1.2.3   Computed Tomography

Image slices from a rotating X-ray source and detector

Computed tomography (CT) uses X-ray images taken around a single axis of rotation to generate multiple slices — *tomographic images* — of the human body.[58] Cardiac CT can be used to assess cardiac anatomy, systolic function, perfusion, viability, coronary artery calcification and to perform noninvasive coronary angiography. CT was invented in 1972 by the English electrical engineer Godfrey Hounsfield. Hounsfield and the American physicist Allan Cormack shared the 1979 Nobel Prize in Medicine or Physiology for their discovery.

Similar to an X-ray fluoroscope, a CT scanner has an X-ray source and one or more detectors. The CT scanner differs in that the source and detector are mounted vertically and opposing each other inside a doughnut-shaped shell — a *gantry*. The patient lies on a table which is automatically fed through the middle of the gantry while the source and detector rotate around the patient, thereby acquiring the image data. Electron beam CT (EBCT) is a less common subtype of CT where the X-ray source is rotated electromagnetically instead of mechanically.

Hounsfield units. The source of signal in a CT images is the tissue *attenuation* of X-rays which is proportional to the density of the tissue. The attenuation is displayed using an absolute scale ranging from -1024 to +3071 *Hounsfield units* (HU). Water has an attenuation of 0 HU, while air has -1000 HU and bone +400 HU.

ECG. A prerequisite for cardiac CT is the simultaneous acquisition of CT image data and ECG data. In this way, image data acquired during different

sequential heart beats can be reconstructed to one set of images that were all acquired at the same phase of the cardiac cycle. Furthermore, the amount of X-ray exposure can prospectively be modulated in relation to the ECG for purposes of minimizing radiation exposure.

Contrast enhanced CT

CT uses the same iodinated contrast medium that is used for other X-ray modalities. The contrast medium is used to enhance the blood pool which is necessary for imaging the coronary arteries, distinguishing the cavities of the heart from the myocardium, and also for assessment of the myocardium as such.

Resolution

Number of channels. An important characteristics of a cardiac CT scanner is the number of detectors or *channels*. A greater number of channels has made it possible to image with a slice thickness which is equivalent to the in-plane resolution. Acquisition of *isotropic voxels* in this fashion makes it possible to reformat three dimensional image stacks in any plane with preserved in-plane resolution. As of 2005, the clinically available state-of-the art CT scanners have 64 channels and yield an effective spatial resolution of 0.6×0.6×0.6 mm.[59]

   Rotation time. The speed of the rotation of the source and detector is called the gantry *rotation time*. The rotation time dictates the temporal resolution of CT. The time to acquire a CT image is roughly half of the rotation time since the reconstruction of one image requires data from just over 180° of rotational transmission. The current 64 channel CT scanners have a rotation time of 330 ms and thereby a temporal resolution of approximately 170 ms.

   Time resolved ECG-gated cardiac CT images can be reconstructed using a *sliding window*. This is typically performed when reconstructing images for assessment of LV volumes and EF. The sliding window approach makes it possible to reconstruct images every 125 ms or less. However, each image which is reconstructed represents information from a duration of acquisition equal to the true temporal resolution, typically 170 ms or more.

Technical strengths and limitations

Cardiac CT has the advantage of being an imaging modality that is accessible at a reasonable cost and with a short study duration. CT has excellent spatial resolution and provides images with signal intensities that are quantifiable on an absolute scale (HU).

Cardiac CT has a relatively poor temporal resolution and is limited by its use of ionizing radiation. Successful imaging is difficult in patients with arrhythmias or severe obesity.

1.2.4 Myocardial perfusion single photon emission computed tomography

Imaging the emission of photons from an injected radioactive substance

Myocardial perfusion SPECT (MPS) is a nuclear medicine technique for imaging the perfusion of the myocardium by intravenous injection of a *radioactive tracer* and subsequent tomographic imaging with a *gamma camera*.[60] Myocardial perfusion can be assessed by MPS both under resting conditions and under exercise or pharmacological stress.

Gamma camera, gamma rays, X-rays and photons

The gamma camera, or scintillation camera, is essentially a photon detector and it was originally invented in 1957 by the American electrical engineer and biophysicist Hal Anger. As previously mentioned, CT relies on an external X-ray source which is *transmitted* through the body and detected on the other side. By contrast, SPECT relies on the injection of a radioactive tracer which *emits* photons − gamma radiation − from inside the body for detection by the gamma camera. Gamma rays and X-rays are both terms used to describe electromagnetic radiation of overlapping wavelengths, and both are called photons. The distinction between the terms depends on the source and not the wavelength. X-rays are generated by energetic electron processes and gamma rays are generated by transitions within atomic nuclei.

Radioactive tracers

The radioactive tracer is the sole source of signal in SPECT images. The biological properties of the radioactive tracer determine where the tracer is deposited or distributed in the body, and thereby what structures or functions are imaged. For this reason, proper interpretation of SPECT images requires knowledge of the radioactive tracer which has been used, and an understanding of its biological properties.

MPS is typically undertaken using one of three different radioactive tracers: ^{201}thallium thallous chloride (^{201}Tl), ^{99m}technetium 2-methoxy-isobutyl-isonitrile (^{99m}Tc-MIBI) or ^{99m}technetium 1,2-bis[bis(2-ethoxyethyl) phosphino] ethane (^{99m}Tc-tetrofosmin). Both ^{201}Tl and ^{99m}Tc tracers are readily extracted

from the blood by cardiac myocytes. This extraction rate is linearly related to blood flow. Their myocardial distribution therefore reflects a function of both the number of myocytes and tissue perfusion.

An additional biological quality of importance is the redistribution of the tracer following injection. ^{201}Tl is a potassium analogue and is readily redistributed into the blood stream whereas the ^{99m}Tc tracers are both nearly irreversibly extracted from the blood stream during the first minutes following intravenous injection.

The redistribution of ^{201}Tl makes it possible to perform viability assessment with ^{201}Tl by imaging immediately at rest and upon subsequent redistribution. Resting perfusion defects which show ^{201}Tl uptake upon late redistribution are thereby considered hypoperfused but viable. ^{201}Tl injection can also be undertaken by imaging after stress, redistribution and reinjection. Stress and redistribution images are taken for the assessment of ischemia, and images taken following reinjection are assessed for viability.[61]

Stress

Epicardial coronary artery stenosis does not always induce limitations in flow under resting conditions. Therefore, assessment during exercise or pharmacological stress is routinely performed. The non-redistributing quality of ^{99m}Tc tracers make it possible to inject the tracer at the time of peak stress which is undertaken outside the gamma camera. Imaging can then be undertaken in the gamma camera a short time later. Conveniently, the distribution of the tracer will be the same at the time of imaging as it was as the time of injection during peak stress. The duration between exercise and imaging is more crucial for ^{201}Tl, considering that it is more readily redistributed.

Exercise stress is ideally undertaken since it mimics the physiological circumstances under which patients experience ischemic symptoms. However, exercise stress may not always be practically possible in patients with reduced mobility. In these cases, pharmacological stress in MPS imaging is routinely undertaken using intravenous infusion of either a vasodilator such as adenosine or its precursor dipyridamole, or the less commonly used β1-receptor agonist dobutamine with or without the addition of atropine. Exercise stress induces a twofold increase in myocardial blood flow. By comparison, the use of a vasodilator induces a fourfold increase in blood flow in normal myocardium. Myocardium perfused by a stenotic artery may not be capable of adequate vasodilation whereby a relatively lesser increase in blood flow upon vasodilation can be visualized as a perfusion defect.

Resolution

Similar to CT, SPECT involves the reconstruction of image slices from data acquired from multiple angles covering 360° around the body. In SPECT, one or more gamma camera detector heads are rotated around the patient in order to acquire data for reconstruction of image slices. The gamma camera uses a physical filter — a *collimator* — to only detect photons which hit the detector at a 90° angle. A SPECT camera detector head is typically 40×40 cm. This makes it possible to acquire data covering the entire heart during a single rotation around the body. However, the speed of rotation is considerably slower than for CT. A typical MPS acquisition uses two detectors mounted at a 90° angle to simultaneously perform 50 seconds of acquisition repeated 32 times over 5.6 degree intervals. This yields a total acquisition time of over 26 minutes.

The spatial resolution in SPECT is limited by physical properties of photons traveling through tissue. When a photon is emitted from an atom as a result of radioactive decay it travels in a straight path. Photon attenuation can occur along this path in the form of either absorption or scatter. Scatter changes the course and affects the energy of the photon. Scattered photons which are detected by the gamma camera are falsely attributed to a position from which they did not originate. The accuracy for the spatial position of photons detected by SPECT is limited to 10 mm. The effective spatial resolution is therefore 10×10×10 mm, and this is typically reconstructed and displayed with a digital resolution of 5×5×5 mm. Aside from the physical limitations of SPECT, MPS images represent an averaged picture from 20+ minutes of free breathing with a beating heart. Blurring from such physiological movement also contributes to the limitation of the spatial resolution of MPS.

As mentioned, the temporal resolution of MPS is on the order of 20 minutes for non-time-resolved images used to assess myocardial perfusion. However, MPS images can also be used to assess LV end-diastolic volume (EDV), end-systolic volume (ESV), stroke volume (SV) and EF. This is performed via automated detection of the contours of the LV using time resolved images from ECG gated acquisition, otherwise called gated MPS. This contour detection does not require the same image quality as is required by the assessment of perfusion. Hence ECG-gated acquisition is routinely performed and yields robust and automatic quantification of LV volumes and EF. The temporal resolution of these images is a trade-off between signal and noise. Typically, gated acquisition allows sufficient border detection when using images reconstructed at 1/8 or 1/16 of the cardiac cycle, yielding a temporal resolution at a heart rate of 60 beats per minute of 125 or 62.5 ms, respectively.

Technical strengths and limitations

MPS is a technique that is routinely used for the clinical assessment of myocardial perfusion and LV function. Relative perfusion can be assessed visually and quantitatively. Gated MPS is readily used to assess LV volumes and EF.

MPS has a limited spatial and temporal resolution and can be prone to artifacts. Due to the limited spatial resolution, accurate assessment of perfusion may be hampered by regional reduction in wall thickness or regional function.[62, 63] In particular, attenuation poses a problem in obese patients. Promising recent advances have shown that attenuation correction based on combined acquisition of CT images offers improved visual and quantitative accuracy.[64]

1.2.5 Positron emission tomography

Imaging using positron emitting isotopes

Positron emission tomography (PET) is a nuclear medicine imaging technique which can be used to quantitatively assess myocardial perfusion and metabolism. PET was developed in 1973 by a team led by Edward J. Hoffman and Michael Phelps at Washington University in St. Louis, Missouri, USA.

PET is similar to SPECT in that both involve detection of a radioactive tracer which typically is injected into the blood stream. However, PET differs from SPECT in two important ways.

Firstly, the radioactive tracers used in SPECT emit single photons, while the radioactive tracers used in PET are isotopes which decay by emitting a positron. The emitted positron travels up to a couple millimeters and then collides with an electron in a process that is called annihilation. The annihilation generates two photons which are emitted in $180°$ opposite directions. The detection of the positron emitting isotope is indirectly achieved by simultaneous or *coincident* detection of the two photons by a detector ring which surrounds the object being studied. The detector ring typically has 500 detectors distributed over $360°$. Photons which are detected at the same time are thereby known to have been emitted from a source along a straight line between the two locations of simultaneous detection. The information about coincident detection along many lines in space are used to reconstruct an image.

Secondly, PET imaging is typically undertaken with a separate scan for transmission in order to apply attenuation correction. Also, with coincidence detection of two photons, the probability of attenuation along the line between the two detectors is uniform. Attenuation correction therefore makes it possible to assess tracer amounts quantitatively.

Radioactive tracers

PET imaging is typically undertaken with radioactive isotopes such as ^{11}C, ^{13}N, ^{15}O, ^{18}F and ^{82}Rb. These isotopes can either be chemically incorporated into biologically relevant compounds which are administered intravenously, or the isotope can be injected as such. PET myocardial perfusion is typically undertaken using ^{13}N-ammonia or ^{82}Rb whereby myocardial blood flow can be quantified in ml/g/min. PET assessment of myocardial metabolism is undertaken using the glucose analogue ^{18}F-fluorodeoxyglucose (^{18}FDG) and glucose utilization can be quantified as g/min per g of myocardium.

Resolution

The spatial resolution in PET is mainly limited by the size of the individual detectors in the detector ring. This typically yields an effective resolution of 5×5×5 mm which typically is reconstructed and displayed with a digital resolution of 2.5×2.5×2.5 mm.

 The PET detector in modern scanners cover at least 15 cm in the feet-head direction. As with SPECT, this makes it possible to acquire image data from the entire heart simultaneously without moving the table. The duration of acquisition for one table position covering the entire heart is typically 5-20 minutes depending on the tracer. PET imaging is undertaken in free breathing and perfusion or metabolism is typically displayed as images representing the average of all movement due to breathing and cardiac pumping. In this sense, PET has a similar temporal resolution when compared to SPECT. Furthermore, ECG-gated acquisition make it possible to reconstruct time-resolved images for quantification of ventricular volumes and EF using similar methods and yielding the same temporal resolution as for SPECT.

Technical strengths and limitations

PET is considered the reference standard for non-invasive quantitative assessment of absolute myocardial blood flow and metabolism. This quantitative capability is attributed to accurate attenuation correction. Although relative perfusion can be assessed using other imaging modalities, PET is the only technique which has a tracer which can be used to assess myocardial glucose utilization (^{18}FDG).

 Moreover, there are a broad range of positron emitting isotopes which can be chemically incorporated into compounds with physiologically relevant properties. An advantage with PET is therefore the potential to develop tracers dedicated to detection of well-defined molecular mechanisms. This has been termed *molecular imaging* and future development in this field is anticipated.

Additional developments include the integration of CT into combined PET-CT scanners. This integration offers the possibility of improved attenuation correction and the simultaneous acquisition of anatomical and functional images in addition to the cardiac diagnostic capabilities of CT.

Limitations for PET imaging include the limited spatial and temporal resolution, ionizing radiation, availability and cost. Availability and cost are influenced by the need to have a cyclotron for production of the majority of positron emitting isotopes. Furthermore, PET involves the use of ionizing radiation and the half lives for cyclotron produced isotopes ranges between 10 min for ^{13}N and 110 min for ^{18}F. These half lives limit the distance of transport from a cyclotron facility.

1.2.6   Magnetic resonance imaging

Using a magnet and radio waves to image protons

Magnetic Resonance Imaging (MRI) uses a strong magnet and radio waves to manipulate the magnetic field associated with hydrogen nuclei (protons) and to measure a signal from which images can be generated. The physics behind MRI has generated several Nobel prizes. Most recently, the American chemist Paul Lauterbur and the English physicist Sir Peter Mansfield shared the 2003 Nobel Prize in Medicine and Physiology for their discoveries in the 1970's concerning MRI.

An MRI scanner has three main components necessary for generating images: a magnet, radio frequency (RF) coils, and a gradient system. Similar to CT and PET scanners, the MRI scanner itself typically looks like a doughnut.

The magnet. The magnet is typically superconducting and consists of metal wire wrapped around the hole in the doughnut-shaped gantry. The wiring is continuously cooled with liquid Helium to $-270°$ C to retain its superconducting state. An electrical current is applied through the wire, thereby generating a very strong magnetic field. The strength of the magnetic field in clinical MRI scanners typically ranges between 0.1 and 3 Tesla (T). Signal-to-noise (SNR) increases with increasing field strength. However, higher SNR at higher field strengths is also partially counterbalanced by the introduction of other limitations. The current standard for cardiac MRI is 1.5T. By comparison, a household refrigerator magnet has a magnetic field strength of 0.01 T and the earth's magnetic field has a strength of approximately 0.00005 T or 50 μT.

From quantum physics, it can be shown that certain nuclei such as hydrogen possess a so-called *spin* resulting in a magnetic moment. Magnetic moments from an ensemble of protons are randomly oriented in space in the absence of an external magnetic field. When the human body is introduced into a strong mag-

netic field, the magnetic moments from protons in the body − *spins* − become aligned with the magnetic field. The spins are approximately evenly distributed in direction, with or against the main magnetic field. There is, however, a slight imbalance of a few more spins per million which point in the direction of the main magnetic field. It is this very small naturally occurring imbalance which is the basis for generating signal in MRI. We will revisit this concept shortly. Furthermore, the spins also begin to rotate − *precess* − around an axis parallel to the magnetic field. The frequency of this rotation or *precession* is called the *Larmor frequency*. The Larmor frequency is different for protons in different molecules and increases linearly with the strength of the magnetic field. Hydrogen in water, for which the Larmor frequency is 42.6 MHz at a magnetic field strength of 1T, is the most abundant atomic nucleus in the human body and hence water forms the basis for MR imaging.

So far, we have hydrogen spins in a magnetic field precessing at a given frequency with a small imbalance in one direction. The small imbalance results in a net *magnetic vector* in the direction of the magnetic field. This net magnetic vector is very small in comparison to the main magnetic field vector. It is virtually impossible to detect when oriented in the same direction as the main magnetic field. However, it is possible to detect this small magnetic vector if it is manipulated so that the direction of the vector deviates at an angle from the direction of the main magnetic field.

The radio frequency coils. RF coils can be used to achieve this desired angular deviation from the magnetic field. An RF coil is another word for an antenna. The RF coil can be used to transmit energy in the form of *RF pulses* into the body while it is inside the MRI scanner. This transmission of RF pulses is performed with a *transmitter coil*. It is important to note that the RF pulse only affects a given spin if it is transmitted at the precession frequency, the Larmor frequency. Hence, spins associated with water protons in a 1T magnetic field can be selectively manipulated by RF pulses which are transmitted at a frequency of 42.6 MHz. The RF pulse and the spin precession are thereby in *resonance*. This is the resonance which is the source of the term magnetic resonance imaging.

The transmission of RF pulses causes the small net magnetic vector described above to deviate at an angle from the direction of the main magnetic field. The component of the net magnetization vector which is oriented perpendicular to the main magnetic field generates a signal current which can be detected by an antenna − an RF *receiver coil*. This signal which is detected by the receiver coil is proportional to the number of protons being studied. In the case of hydrogen in the human body, the signal is practically proportional to the water content in the tissue.

In summary, the signal in MRI is detected by the receiver coil. The signal is generated by spins rotating at their Larmor frequency, which have been deflected

at an angle from the main magnetic field by an RF pulse generated by the transmitter coil. This explains the source of the signal, but it does not explain how MRI can be used to spatially locate the signal and generate images representing only tissue in a defined slice through the body.

The gradient system. A gradient system is used to spatially locate the signal in MRI. The gradient system is composed of *gradient coils* which can generate linear variations − *gradients* − in the main magnetic field. An MRI gradient is typically 1% of the main magnetic field strength. As previously stated, the Larmor frequency is linearly proportional to the magnetic field strength. Thus, a gradient in the magnetic field will result in different resonance frequencies for water protons at different positions in the magnetic field. A *slice selective gradient* can then be applied by the gradient coils so that an RF pulse with a given frequency only excites the protons resonating at a given frequency in a given slice. The imaging plane can be positioned and angled arbitrarily in all three spatial dimensions.

The gradient system is thus used in combination with the transmission of RF pulses to define the slice from which signal is generated. After slice selection, the gradient system is also used to encode the signal in the x and y direction. A gradient in the y direction can be applied prior to signal detection to induce differences in spin frequency, causing a phase shift which remains during the detection of the signal. The creation of this phase shift in the y direction is termed *phase encoding*. Furthermore, a gradient can be applied during the signal sampling to induce differences in frequency in the x direction, a procedure known as *frequency encoding*. Phase and frequency encoding in this manner can be used to spatially localize the unique position of the signal in both the x and y direction within the selected slice.

The raw signal data is acquired in the frequency domain, or *k-space*. In k-space, signal information is encoded using phase and frequency information. When a signal is sampled, the information which is measured is typically comprised of one line of raw data, a line in k-space. The raw data image is generated through sequential and repeated acquisition of a sufficient amount of lines in k-space. The number of lines which are acquired in combination with the number of sampling points in the sampled signal determines the spatial resolution in the final image. Finally, the raw data in k-space can be transformed into an anatomical image using a mathematical operation called Fourier transformation.

In summary, an image is acquired by applying gradients and RF pulses for slice selection, phase-encoding and frequency encoding. The timing schedule describing this process is known as a *pulse sequence*. The different characteristics of a pulse sequence can be manipulated in the scanner software by the user to achieve desired image characteristics.

T1 and T2 relaxation

The signal in MRI has been described above as being generated by hydrogen nuclei in water. Moreover, there are two principally different and important aspects of the MR signal which are called *T1 relaxation* and *T2 relaxation*.

It has previously been mentioned that an RF pulse is used to deviate the net magnetic vector at an angle from the main magnetic field. Let us visualize the magnetic vector as an arrow pointing along the vertical axis in a diagram with a vertical and a horizontal axis. The vertical axis represents the direction of the main magnetic field. In the case of an RF pulse which induces a 90° angle of deviation, or *flip angle*, the magnetic vector will be flipped horizontally. After the 90° RF pulse, the magnetic vector will be subject to *relaxation*.

Relaxation can be described as a simultaneously occurring two-component process. The horizontal or transverse component of the net magnetic vector will decrease and its vertical or longitudinal component will increase back in the vertical direction. The increase of the vertical component is called T1 relaxation and the decrease of the horizontal component is called T2 relaxation. T1 is a constant which is defined as the time it takes to regain 63% of the original magnetization in the vertical direction. T2 is defined as the time it takes to decrease to 37% of its value immediately after the RF pulse. T1 in human tissue varies between $300-1500$ ms and T2 varies between $50-500$ ms. An exception from these values is free water, which is associated with significantly higher values of both T1 and T2.

The T1 and T2 relaxation properties of different tissues vary considerably. It is therefore possible to acquire images which are either T1-weighted or T2-weighted in order to differentiate between different tissues.

Contrast enhanced MR

Both T1 and T2 can be manipulated through the use of MR contrast agents. Contrast agents are not necessary for imaging of cardiac function. However, an intravenously administered MR contrast agent is used for contrast enhanced MR angiography and the assessment of myocardial perfusion and infarction. The most common clinically used cardiac MR contrast agent is the element gadolinium (Gd) coupled to the carrier molecule diethylenetriamine penta-acetic acid (DTPA).

The presence of Gd in tissue dramatically shortens T1. Importantly, it is not Gd *per se* which emits a signal. Rather, Gd has a T1-shortening effect on the protons in its immediate surroundings. Also, the distribution of the Gd in the body is determined by the biological properties of the carrier molecule. DTPA is a molecule which freely distributes into the extracellular space throughout the body

and is excreted via the kidneys. Importantly, Gd-DTPA is not taken up intracellularly. Also, allergic reactions to Gd-DTPA are extremely rare and Gd-DTPA can readily be administered to patients with kidney failure without damaging effects.

Function

Cardiac function is assessed by MRI using time-resolved, or *cine*, imaging. Imaging can be performed either in real time or by synchronizing image data acquisition with the ECG. The current clinical routine for cine cardiac MRI is to perform retrospectively ECG-gated image acquisition during a breath hold.

Retrospective ECG-gating involves continuous and simultaneous acquisition of ECG and image data. The process is in principle identical to ECG-gating performed in MPS. Cine cardiac MRI typically requires 5 s of breath hold acquisition to acquire sufficient image data to generate images of a single heart beat in one slice. Cine image acquisition typically involves imaging three consecutive slices during a breath hold of approximately 15 s.

ECG. The strong magnetic field in MRI distorts the ECG, sometimes making it difficult to automatically detect the R wave. Vectorcardiography (VCG) is readily used since it provides a reliable ECG signal when the patient is in the scanner. The terms VCG and ECG are used synonymously in this sense.

Recent developments have been made whereby it is possible to acquire information on cardiac phase directly from the raw image data. This technique is called self-gating and has been shown to produce results which are indistinguishable from ECG-gated images.[65, 66]

Furthermore, it has been shown that simultaneous respiratory and cardiac self-gating can be achieved using the same principle of extracting information on movement from raw image data.[67] These developments show promise in eliminating the need for breath hold acquisition with an ECG signal of sufficient quality for gating. However, they have not yet been implemented in clinical scanners from all major manufacturers. Importantly, all forms of gated acquisition require a regular cardiac rhythm. Arrythmias therefore pose a problem.

Single slice real time imaging without gating can be performed using a technique called *k-t* BLAST. Single slice *k-t* BLAST can be performed with an acceptable spatial resolution and a temporal resolution of 27 ms,[68] and can also be used to perform 3D cine imaging of the entire LV in one breath hold. The *k-t* BLAST technique shows promise for real time imaging. However, the technique awaits implementation and evaluation in clinical scanners.

Sequences. The sequence currently used in clinical routine for assessing cardiac function using cine MRI is a steady state free precession (SSFP) sequence. The signal in SSFP images can be said to reflect the ratio between T2 and T1. An SSFP sequence generates images in which the blood appears bright and the myo-

cardium appears dark grey. No contrast agent is necessary to achieve excellent contrast between blood and myocardium.

It is also possible to assess regional myocardial function using a grid tag sequence. In grid tag imaging, the signal in the tissue is intentionally nulled in a grid pattern throughout the image. This grid-patterned signal nulling is performed at the start of the cardiac cycle. Images can then be acquired throughout the cardiac cycle whereby the deformation of the myocardium can be appreciated as deformation of the grid. Additional techniques for assessing regional myocardial function have been developed and will be discussed in brief later on.

Perfusion

Myocardial perfusion can be assessed using MRI by imaging the myocardium sequentially during the simultaneous intravenous injection of an MR contrast agent such as Gd-DTPA. Typically, 3-8 short axis slices are imaged once per cardiac cycle during the first pass of the contrast agent through the LV myocardium. Normally perfused myocardium increases rapidly in signal intensity as the contrast agent enters the myocardium. Hypoperfused myocardium may appear hypoenhanced due to the delayed arrival of contrast in myocardium that is perfused by a coronary artery with a flow-limiting stenosis. The time it takes for the myocardium to enhance during first pass imaging can be assessed visually or quantitatively as the upslope of the signal intensity over time.

Infarction

MRI can be used to image myocardial infarction by commencing imaging 10-20 minutes after the injection of an extracellular contrast agent such as Gd-DTPA. The technique is called *delayed enhancement* because of the delay between contrast injection and imaging.

Contrast physiology. Intravenously injected Gd-DTPA is distributed according to its distribution volume in different tissues. Gd-DTPA in blood is distributed in the plasma which comprises approximately 50% of the volume. In normal myocardium, Gd-DTPA is distributed in the extracellular space which comprises 20% of the volume. Acute infarction is defined by the irreversible rupture of the myocyte cell membrane. Upon rupture, the extracellular space in infarcted myocardium becomes contiguous with the intracellular space prior to the rupture of the cell membrane. Gd-DTPA in acute infarction is distributed in this extracellular space which comprises 80-90% of the volume.[69] A similarly increased extracellular space is also found in the fibrotic scar tissue of chronic infarction. The considerable difference in distribution volume of Gd-DTPA in viable and non-viable myocardium thereby make it possible to acquire MR images

with sharp contrast between these two. Following injection, it takes approximately 20 minutes before the distribution volume of Gd-DTPA in infarction reaches a steady state.[70]

Sequences. The pulse sequence used for infarct imaging is a T1-weighted inversion recovery sequence.[71] The pulse sequence is adjusted so that viable myocardium appears black and infarcted myocardium appears white. The blood pool appears grey with these same pulse sequence settings. Acute infarction and chronic infarction both appear bright − *hyperenhanced* − when imaged with this pulse sequence.

Importantly, acute and chronic infarction can be differentiated from each other by imaging using a pulse sequence which enhances edema.[72] This sequence is a T2-weighted inversion recovery sequence and it must be undertaken prior to contrast injection. Edema in acute infarction can be imaged starting the day after infarction. Chronic infarctions older than three months show no signs of edema.[73]

Flow and velocity encoding

Flow quantification using MRI is highly accurate and is routinely used to quantify flow in the great vessels for measurement of stroke volume, cardiac output, shunt and for direct and indirect quantification of valvular regurgitation.

Flow is generally quantified by first selecting an imaging plane perpendicular to the vessel of interest. The images are then acquired with a pulse sequence which permits *velocity encoding* of the image. The velocity encoded information in MRI is analogous to velocity information from Doppler in echocardiography.

When using velocity encoded MRI, the result of the MRI scan is two sets of images for each time point in the cardiac cycle. One is an anatomical image and the other is an image where the signal intensity in each pixel is directly proportional to the through-plane velocity. The average velocity in a vessel is hence quantified by measuring the average signal intensity for each pixel in the cross section of the vessel, and then multiplying by a known constant. The flow is calculated by multiplying the mean velocity by the cross-sectional area of the vessel. This flow data can be used to graph flow versus time. The area under the flow versus time curve for one cardiac cycle is the stroke volume.

Velocity encoded flow quantification by MRI is very robust in large vessels. However, measurement in smaller vessels such as the coronary arteries or the coronary sinus can be challenging. The movement of the vessels and the limited spatial and temporal resolution introduce uncertainties into such measurements.

Velocity encoding can also be used to measure velocities in more than one direction and in tissues other than blood. In-plane velocity encoded quantification of the velocities of myocardial movement have been used to calculate two-

dimensional myocardial strain. The potential of such measures to quantitatively assess regional myocardial function are currently being evaluated.[74]

Coronary angiography

Magnetic resonance imaging can be used to perform coronary angiography. The duration of image acquisition must currently exceed the duration of a breath hold in order to achieve sufficient spatial resolution. Therefore, imaging is typically undertaken during free breathing. Image acquisition is only performed in end-expiration with the help of a *navigator echo*. A navigator echo is used to acquire one-dimensional images over the diaphragm in order to determine its position throughout the respiratory cycle.

MR coronary angiography can be performed without intravenous contrast using two principally different sequences. The most common approach uses a bright blood SSFP sequence.[75] However, it is also possible to use a black blood sequence for assessment of the thickness of the coronary artery vessel wall.[76]

Resolution

MR imaging involves a trade off between spatial resolution, temporal resolution and the duration of image acquisition. For example, *ex vivo* imaging of the non-moving heart can in theory be undertaken with image acquisition durations of hours and a spatial resolution of $0.1 \times 0.1 \times 0.1$ mm. By comparison, MR coronary angiography in patients typically requires up to 20 minutes of free-breathing image acquisition to achieve a spatial resolution of $1 \times 1 \times 1$ mm for a data set with a temporal resolution of approximately 100 ms.

Five seconds of breath hold imaging of LV function with an SSFP sequence typically yields a single slice with a spatial resolution of $1.2 \times 1.2 \times 8$ mm and a temporal resolution of 30 ms. A temporal resolution of 15 ms can readily be achieved by doubling the duration of image acquisition to a 10 s breath hold. However, this is not done in clinical routine since a 30 ms temporal resolution is more than physiologically adequate for the clinical assessment of regional and global LV function.

Technical strengths and limitations

MRI is a versatile technique for assessing cardiac anatomy and physiology. It has no known harmful effects on the human body and can be undertaken repeatedly in the same subject without considerations of exposure to ionizing radiation. MRI is used to acquire images of a wide range of soft tissue contrasts without restraints regarding positioning of the imaging plane. MRI is the reference standard for *in vivo* determination of LV volumes, EF, flow quantification in large vessels and

infarct size. The technology as such is constantly undergoing development and there is no reason to believe that these developments have reached a plateau.

However, MRI has some important limitations. Patients with pacemakers are currently not routinely scanned because of several risk aspects, including the potential for the RF pulses or the imaging gradients to induce currents in the pacemaker leads. Exceptions have been made and patients with pacemakers have successfully been scanned after thoroughly weighing the risks and potential benefits of the investigation.

All ferromagnetic implants pose at a minimum a problem in that they cause localized imaging artifacts. There is also a risk that an MRI examination may induce movement in or heating of an implant. Sternal wires and coronary stents fortunately only cause localized artifacts and are otherwise safe to image.

Claustrophobia is a significant concern which stands in the way of imaging in between 2-5% of patients, more than half of which can be successfully scanned under light sedation.[77]

1.3   Non-invasive imaging in the assessment of ischemic heart disease

There exists considerable overlap between the ability to assess different anatomical and physiology aspects of IHD using different cardiac imaging modalities. Certain modalities are particularly favorable for the assessment of specific parameters. This section will present an overview of the relative utility of different modalities for these different assessments with a focus on MRI and SPECT. A summary of these properties is presented in Table 1.3.

1.3.1   Myocardial function

MRI is considered the reference standard for assessment of global and regional function.[78] This section will cover the assessment of systolic myocardial function. Diastolic function can also be assessed but this will not be covered.

Global function. MRI measures LV volumes accurately without the use of geometric assumptions,[79,80] and with an excellent interstudy reproducibility[81–84] which is superior to 2D echocardiography.[85] Assessment of LV volumes by 3D echocardiography has shown a very close correlation and minimal mean bias when compared to MRI.[86] When compared to LV volumes and EF by MRI, an excellent correlation has been found for gated SPECT,[87–96] gated PET[97–101] and gated CT.[96,102,103] However, measurements of LV volumes with gated SPECT and gated PET have been shown to have a considerable variability, whereas CT

TABLE 1.3
Relative utility* for assessing different physiological parameters
with different cardiac imaging modalities

	Function	Perfusion	Viability	Coronary stenosis	Cost
Echo	+++	++	++	+	$
X-ray	+	-	-	++++	$$$$
CT	++	+	+	+++	$$
SPECT	++	+++	++	-	$$
PET	++	++++	+++	-	$$$
MRI	++++	++	++++	++	$$

* Relative utility is a composite suggestion based on relative merits of resolution, validation, reproducibility and diagnostic accuracy.
+ denote a relative scale where greater number of + indicate greater utility.
$ indicate increasing costs.

has been shown to have a lesser variability than both SPECT and 2D echocardiography when compared to MRI.[96]

Regional function. Wall thickening by MRI can readily be used to assess regional function[104, 105] with good agreement between visual and quantitative assessment.[106] Echocardiography is used to visually assess regional systolic function[107] and additional techniques such as M-mode and myocardial Doppler imaging are also available.[108] Similarly, X-ray fluoroscopy has been used to invasively assess regional function.[109] Furthermore, regional function can also be assessed by gated SPECT,[87–89, 91] PET[100, 101] and CT[103] with good agreement compared to MRI. Wall thickening has been shown to be better than wall motion for the assessment of regional systolic function.[110] For example, assessment of regional function by X-ray fluoroscopy shows a gradient in normal wall motion from the base to the apex[111] which is not present for wall thickening by MRI.[105]

Regional function may also be assessed by measuring strain in the myocardium. Quantification of strain can be performed in any direction using MRI grid tagging[112] or MRI velocity encoded imaging.[74] Notably, strain from grid tagging has been shown to be more sensitive for detecting regional dysfunction compared to wall thickening.[113] Also, echocardiography can be used to assess strain rate,

although limited to assessment in the direction of the scan lines using myocardial doppler imaging.[114]

1.3.2   Detection of coronary artery disease

Perfusion

MPS. The importance of assessing perfusion in the detection of CAD is paramount. Numerous studies have shown that the risk of cardiac events increases with the extent and severity of perfusion defects assessed by MPS.[115] Furthermore, the number of lives saved due to treatment with revascularization compared to medical treatment increases with the amount of ischemic myocardium identified by MPS.[116]

Pooled analysis of 79 studies (8964 patients) using MPS to detect CAD by invasive angiography showed a weighted mean sensitivity of 86% and specificity of 74%.[8] Of patients with normal MPS studies, only those with a high suspicion for CAD are referred for invasive coronary angiography. Therefore, the relatively low specificity for MPS may reflect such a referral bias. The percentage of normal MPS studies in a population with a low likelihood of CAD is called the *normalcy rate*. Normalcy is thereby a better descriptor of the performance of a test in a population without disease. The normalcy rate for MPS in 10 studies (543 patients) was 89%.[8]

PET. PET is considered the reference standard for assessing myocardial perfusion and it accurately identifies reduced perfusion due to stenosis in animals[117] and patients.[118] However, due to the limited availability and high cost of PET, MPS is performed in a far higher volume in clinical practice.

Echocardiography. Perfusion may also be assessed using myocardial contrast echocardiography (MCE) using microbubbles.[119] Experienced centers have reported an excellent agreement between MPS and MCE for detecting perfusion abnormalities, yielding a comparable accuracy for detecting CAD.[120, 121] By comparison, others have shown a 62% head-to-head agreement between MPS and MCE which improved to 82% when excluding attenuation artifacts.[122]

MRI. MRI has an emerging role in the assessment of perfusion. Quantitative analysis of first pass contrast kinetics has been used to identify stenosis by invasive coronary angiography and has been shown to correspond to perfusion by PET[123] and perfusion by microspheres.[124] Visual assessment of perfusion for detection of stenosis has shown a sensitivity of 91-93% and a specificity of 62-75%.[125, 126] The results of a multicenter multivendor trial including head-to-head comparison with MPS are anticipated in the near future.

CT. CT has been used to assess myocardial perfusion, showing similar results when compared to MPS.[127] Perfusion defects appear as regions of hypoenhance-

ment immediately following contrast injection. The kinetics of the contrast cannot be repeatedly imaged without considerable radiation exposure and this is a limitation. Nonetheless, CT imaging performed at rest immediately following contrast injection as part of a CT coronary angiography protocol has shown a sensitivity of 50% and specificity of 92% to detect perfusion defects which are visible at stress using MRI.[128]

In summary, the overwhelming majority of clinical evidence for accuracy and prognostic information from perfusion assessment has been undertaken using MPS. PET is the reference standard and both MRI and echocardiography are promising techniques which have not yet been fully established in routine clinical practice.

Myocardial function at stress

Both MRI and echocardiography can readily be used to assess systolic function during stress. In accordance with the ischemic cascade, a reduction in regional myocardial function at stress is a sign of ischemia and indicative of the presence of CAD. Also, assessment of global function following stress is often routinely performed using MPS.

Echocardiography. Pooled analysis of 15 exercise stress echocardiography studies (1849 patients) shows a weighted sensitivity of 84% and specificity of 82% for detection of CAD.[129] Dobutamine stress echocardiography showed a sensitivity of 80% and specificity of 84% in 28 studies (2246 patients).[129]

MRI. Ten studies (654 patients) using dobutamine stress MRI show a sensitivity and specificity of 89% and 84%.[126, 129] In head-to-head comparison with echocardiography, MRI has shown a better sensitivity and specificity.[130] Furthermore, MRI has shown better image quality and an accuracy that is not sensitive to image quality, as opposed to echocardiography.[131] Head-to-head comparison between dobutamine stress assessment of function and adenosine stress assessment of perfusion has been undertaken using MRI. This study has shown that functional assessment using dobutamine has similar sensitivity but better specificity compared to adenosine perfusion.[126]

MPS. Assessment of EF using gated SPECT in addition to perfusion gives added information in the diagnosis of CAD. Gated SPECT reduces the number false positive tests from 14% to 3%,[132] the number of inconclusive tests is reduced from 31% to 10%, and the normalcy rate improves from 74% to 93%.[133] Furthermore, pooled data show that cardiac event rate increases exponentially as post stress EF by gated SPECT decreases.[134]

In summary, stress induced systolic dysfunction occurs later in the ischemic cascade compared to reduced perfusion. Despite this, detection of stress induced systolic dysfunction appears equally sensitive and more specific than detection

of reduced perfusion for the identification of significant coronary stenosis. MRI is the reference standard for assessment of myocardial function at stress whereas echocardiography is more readily utilized in clinical routine, mostly due to increased availability and lesser cost.

Coronary stenosis

X-ray fluoroscopy is the invasive reference standard for the assessment of coronary artery stenosis. Moreover, non-invasive imaging with both CT and MRI can be used to assess coronary anatomy and stenosis.

When attempting non-invasive imaging of the coronary arteries with either CT or MRI, it should be kept in mind that coronary arteries move throughout the cardiac cycle and ideally require imaging with a temporal resolution of <33 ms as is readily achieved with X-ray fluoroscopy. It has been shown that there is a common period of <1 mm movement of all coronary arteries in late diastole.[135] The duration of this period ranges between 66-330 ms and is on average 187 ms. This indicates that although a temporal resolution of 170 ms is sufficient for imaging most patients' coronary arteries, there are still many patients where blurring due to movement will pose a problem.

CT. Despite the challenges posed by limitations in spatial and temporal resolution, CT coronary angiography has shown promise. Recent studies using 16 channel scanners have shown sensitivities between 82-95% and specificities between 86-98%. The recently introduced 64 channel scanners have shown a sensitivity of 94-95% and specificity of 86-97% with 0-12% segments excluded from analysis.[59, 136] Notably, the negative predicted value was 98% for both studies, indicating the potential for using CT to accurately exclude stenosis in patients with a low likelihood for CAD. Limitations include the inability to assess arterial segments which are calcified or exhibit insufficient image quality due to vessel motion artifacts, and the inability to perform multiple examinations in the same individual due to radiation exposure.

Furthermore, coronary artery calcification as measured by CT has been studied extensively and shown to provide incremental information for risk stratification of patients with suspected CAD.[137] Head-to-head comparison with MPS shows both an increased likelihood of ischemia with increasing calcium score, and significant calcification in the presence of normal MPS findings.[138]

MRI. Data from 28 studies (903 patients) comparing MRI with invasive angiography show a sensitivity of 72%, specificity of 87%, and up to 30% uninterpretable segments.[75, 139] Furthermore, black blood MR coronary angiography has been used to identify increased coronary artery wall thickness in patients with preserved coronary artery lumen diameter and non-significant CAD.[76]

In summary, CT currently outperforms MR coronary angiography with re-

gards to diagnostic accuracy for non-invasive identification of coronary stenosis. Both CT and MRI are currently undergoing continued technical development and further improvements in both technical and diagnostic performance are anticipated.

1.3.3   Myocardial viability

An important challenge in the identification of dysfunctional but viable myocardium is in the determination of myocardial viability. Several non-invasive imaging techniques offer this possibility and they include ^{201}Tl and ^{99m}Tc tracers used for MPS, ^{18}FDG PET, dobutamine stress echocardiography, dobutamine stress MRI and DE MRI.

A comprehensive review of non-MRI techniques for viability assessment was undertaken for 105 studies of just over 3000 patients. In these studies, regional functional improvement following revascularization occurred in 53% of the evaluated segments which were identified as dysfunctional but viable prior to intervention. The overall mean weighted sensitivity and specificity of the techniques was 84% and 69% for identification of regional functional improvement after revascularization.[140] Furthermore, pooled data has highlighted the prognostic importance of viability testing by showing that patients with significant viability which were revascularized showed a greater than 50% reduction in cardiac event rate compared to both those which were treated medically and those without viability who were either treated medically or with revascularization.[141]

PET. Some argue that ^{18}FDG PET should be the reference standard for assessment of myocardial viability.[142] This standpoint is justifiable considering the extensive evidence in the literature. PET has been shown to predict recovery of regional function following revascularization.[143] Pooled analysis from six PET studies showed an average increase of 11% LVEF in patients with dysfunctional but viable myocardium compared to a decrease in 2% LVEF for those who did not.[144] Twenty studies (598 patients) showed a mean sensitivity of 93% and specificity of 58% for predicting functional recovery following revascularization.[140] Furthermore, PET has shown that patients with dysfunctional but viable myocardium which undergo early revascularization show a lower preoperative mortality, greater improvement in post-operative LVEF and higher event free survival compared to those which undergo late revascularization.[145] Also, PET was performed in 67 patients that were initially scheduled to undergo heart transplantation, revascularization or medical therapy. The results of the PET viability scan altered treatment in 46% of patients, thereby illustrating the effect of PET upon clinical decision making.[146]

Echocardiography. Stress echocardiography using low dose dobutamine can be used to evaluate the viability of myocardium which is dysfunctional at rest. The

presence of a significant amount of dysfunctional myocardium which improves in regional function upon stimulation with low dose dobutamine has been shown to predict a lesser cardiac event rate and greater improvement in myocardial function following revascularization compared to patients with little or no dysfunctional but viable myocardium.[147]

Myocardial contrast echocardiography has been applied to identify hibernating myocardium with promising initial results.[148] Also, MCE alone has shown a similarly high sensitivity and low specificity as for MPS. However, when MCE is combined with stress echocardiography it provides improved diagnostic performance.[149]

MPS. Pooled comparison of 11 studies (325 patients) with a head-to-head comparison of ^{201}Tl, ^{99m}Tc and ^{18}FDG versus stress echocardiography for the detection of dysfunctional but viable myocardium has shown that nuclear techniques have a higher sensitivity (90% vs. 74%) but a lower specificity (57% vs. 78%) compared to stress echocardiography.[140] Also, gated SPECT has shown to improve the detection of dysfunctional but viable myocardium.[150] Furthermore, low dose dobutamine has also been combined with gated SPECT to assess contractile reserve and thereby improve the accuracy of detecting dysfunctional but viable myocardium which will improve in function following revascularization.[151]

MRI. Improvement in regional function assessed by low dose dobutamine stress MRI has shown a close agreement with viability by PET[152] and a sensitivity of 89% and specificity of 94% for predicting improvement in function following revascularization.[153] Moreover, assessment using grid tagging and dobutamine has shown a similarly high sensitivity of 89% and specificity of 93% for predicting functional improvement after revascularization.[154]

DE MRI has emerged as a powerful tool for accurate and high resolution assessment of myocardial viability.[155] The technique has been validated showing excellent agreement with histology in animals.[156–158] These data demonstrate the ability of DE MRI to differentiate between viable and non-viable myocardium independent of wall motion, reperfusion status or infarct age. Studies in humans have shown infarct transmurality to be predictive of recovery of regional function following acute infarction,[159,160] revascularization[161–164] and β-blocker therapy.[165] Human studies have demonstrated excellent repeatability[166] and good agreement with both ^{18}FDG PET,[162,167,168] MPS[169–171] and MCE.[172] The assessment of infarct size by MPS, however, can both overestimate[170] and underestimate[169] infarct size by DE MRI. Importantly, one study showed that 47% of subendocardial infarcts identified by DE MRI were missed by MPS,[169] and this is likely attributable to the limited resolution in MPS. Also, DE MRI can be used to definitively assess viability in patients with suspected attenuation artifacts by MPS.[173] The spatial resolution in DE MRI is on the order of 5-10 times greater than MPS and can resolve small peri-procedural infarctions not detected by other

techniques.[174, 175]

Studies comparing low dose dobutamine stress and DE MRI have shown conflicting results. Two studies have shown similar or better results for DE MRI compared to low dose dobutamine when it comes to predicting functional recovery following revascularization.[176, 177] However, other studies have shown that contractile reserve with dobutamine is superior to DE MRI for predicting functional recovery,[178] and may add information particularly regarding the potential for functional recovery of segments with intermediate infarct transmurality.[179] Thus, the relative contributions of contractile reserve and viability by DE MRI to functional recovery and prognostic benefit following revascularization are worthy of further study.[180]

CT. The concept of delayed contrast enhancement of infarcted myocardium which is the established terminology for infarct imaging using MRI was first described using CT in 1980 by Higgins and coworkers.[181] However, the first study in humans to compare infarct size by delayed contrast enhancement CT and MRI was recently performed and showed excellent agreement.[182]

In summary, DE MRI has developed as the reference standard for assessment of the transmurality and extent of infarction. It offers advantages of increased spatial resolution over alternative techniques. In particular, DE MRI is an imaging technique whereby non-viable infarction is imaged directly through an increased tissue distribution volume of contrast in non-viable tissue, as opposed to relying on the absence of signal or subjective analysis of regional function as with nuclear and echocardiographic techniques, respectively. Meta-analysis has shown a lower cardiac event rate for patients with dysfunctional but viable myocardium which are treated with revascularization compared to medical treatment.[45] A major limitation of that study was the potential for selection bias due to the retrospective and non-randomized design of the study. The results of two ongoing prospectively randomized trials (STICH and UK Heart) are eagerly awaited as they are needed to clarify the prognostic value of viability assessment.[183]

Chapter 2

Aims

The general aim of this thesis was to further elucidate the pathophysiology of dysfunctional but viable myocardium in patients with IHD.

Dysfunctional but viable myocardium consists of subgroups defined by distinct characteristics with regards to function, perfusion and viability.

Therefore, we sought to quantitatively compare these parameters and assess to what degree regional function reflects regional infarction, to what degree global function reflects total infarct size, and to determine the time course for recovery of function and perfusion following revascularization in relation to viability.

The specific aim for each paper was:

   I. To develop a method for side-by-side quantitative assessment of myocardial function, perfusion and viability from MRI and SPECT.

  II. To study the relationship between regional function and infarct transmurality.

 III. To study the relationship between global function (LVEF) and infarct size and determine a maximum predicted LVEF in relation to infarct size.

  IV. To study the time course of quantitative changes in regional perfusion and function following revascularization in relation to the presence of infarction.

Chapter 3

Materials and Methods

3.1 Study populations

All protocols and procedures were approved by the ethics committee for human research at Lund University, Sweden. All subjects were recruited at Lund University Hospital. All subjects in Paper I, Paper II and Paper IV provided written informed consent, while the ethics committee provided a waiver of individual consent for the clinical patients in Paper III.

Paper I

Paper I studied prospectively recruited patients with a history of CAD who were scheduled for first time elective CABG. Exclusion criteria for all subjects were absence of sinus rhythm, claustrophobia or contraindications for MRI.

Paper II

For Paper II, inclusion criteria for patients included either elective first time CABG or first time ST-elevation acute myocardial infarction treated with acute PCI. All patients were imaged six months after revascularization of all stenosed vessels. Inclusion criteria for controls included the absence of a history of cardiovascular or systemic disease, blood pressure less than 140/90 mmHg and a normal electrocardiogram.

Paper III

For Paper III, patient inclusion was retrospectively undertaken through review of reports for all patients clinically referred for viability assessment using DE-MRI at

our institution between January 2000 and December 2004. Patients were referred for known or suspected ischemic heart disease or other forms of cardiomyopathy. Patients were only considered if the report from their study included quantification of LVEF, LVM and the volume of infarction. For the purpose of this study, patients were classified as either having IHD, normal findings, or other forms of non-ischemic cardiomyopathy (CM) based both on the information in the referral and the conclusions of the CMR report. Normals were defined as those exhibiting normal functional and morphological results at CMR. Classification into IHD or CM was made according to the CMR report when the report gave a definitive diagnosis using established criteria.[184]

Paper IV

Inclusion criteria for Paper IV were clinical selection for first time elective revascularization by CABG or PCI. Patients were imaged with cardiac MRI and rest/stress SPECT prior to revascularization and one and six months after revascularization. Exclusion criteria were valvular surgery in adjunct to revascularization, acute coronary syndrome during the course of the study, New York Heart Association functional class IV, absence of sinus rhythm, claustrophobia or contraindications for MRI.

3.2   Assessment of perfusion using myocardial SPECT

3.2.1   Myocardial perfusion SPECT imaging

MPS was performed in Paper I and Paper IV using the same protocol. Rest and stress imaging were performed on separate days, 30 minutes after intravenous injection of a body weight adjusted dose (500-700 MBq) of ^{99m}Tc-tetrofosmin. Stress imaging was undertaken using either pharmacological or exercise stress. Pharmacological stress employed 5 mg/ml adenosine infused at a rate of 140 μg/kg/min for 3 minutes before tracer injection, and continued for 2 minutes following injection. Exercise stress was performed using a bicycle ergometer with a minimum increase to 85% of the maximum predicted heart rate.

Subjects were imaged in the supine position with a dual head camera in steps of 5.6 degrees, 32 projections, 50 s/projection, using a 64×64 matrix yielding a digital resolution of $5\times5\times5$ mm. Iterative reconstruction using maximum likelihood-expectation maximization (MLEM) was performed with a low-resolution Butterworth post filter with a cutoff frequency set to 0.6 of Nyquist and order 5.0. No attenuation or scatter correction was applied. Lastly, short and long axis images were reconstructed.

3.2.2 Image analysis

Visual assessment

For visual perfusion scoring, short axis rest and stress SPECT images were assessed independently, blinded to the corresponding rest or stress images and CMR results. Scoring was performed by an experienced reader using a 12 segment per slice, four slice model. An example of the segmental model is illustrated in Figure 3.1. Images were scored using the following scale: 0: normal, 1: mild perfusion abnormality, 2: moderate abnormality, 3: severe abnormality, and 4: maximal abnormality (no perfusion).

Quantitative assessment

For quantitative measurement, the centroid of the left ventricular lumen was defined manually in each 10 mm thick short axis slice at rest and stress from SPECT. Images were manually cropped using a circular selection tool. From the centroid, perfusion was quantified as the area under the count density curve along a radial profile. The visually assessed transition between the myocardium and the blood pool typically ranged between 20-50% of the maximal count density in the same slice. In order to exclude measurement of counts from the blood pool, a cut off value of 30% of the maximal count density in the same slice was therefore chosen as the endocardial limit of the area under the curve measurement for each radial profile. All perfusion values were normalized, where the maximum uptake in the entire LV was set to 100%.

Polar plots

Polar plots for perfusion, function and viability were generated with in-house developed software using the quantification data from each respective modality. All data was treated as polar coordinates (slice number as radius, segment position as angle) and subsequently converted to Cartesian coordinates for graphing as polar plots.

3.3 Assessment of function using cine MRI

3.3.1 MR imaging

All imaging was performed in the long and short-axis planes during end-expiratory apnea using a 1.5T system (Siemens Magnetom Vision, or Philips Intera CV). LV function was imaged using either a prospectively ECG-triggered cine gradient echo sequence (Siemens, spatial resolution 1.6×1.6×8 mm, gap 2 mm, temporal
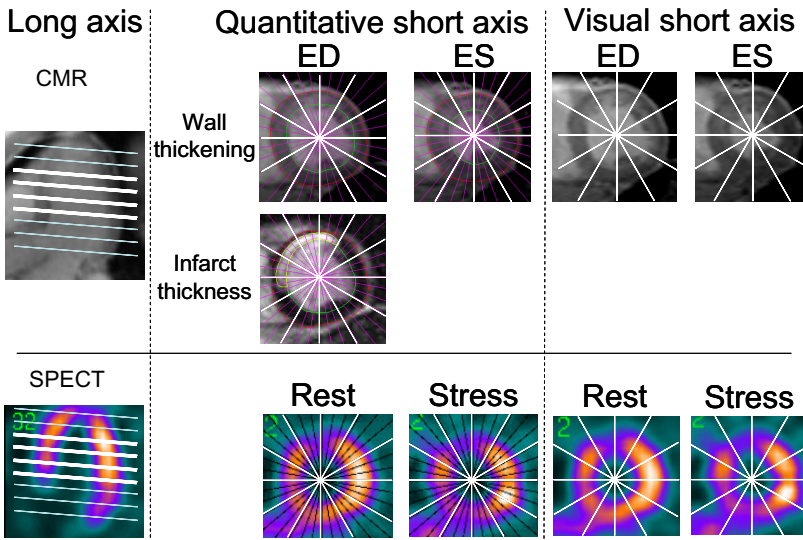
FIGURE 3.1 Alignment of short axis slices between CMR (upper) and SPECT (lower) images. The long axis image of the left ventricle (left) used to plan the appropriate short axis images (middle and right) are shown for both imaging modalities. All LV short axis slices were used to develop polar plots. The middle four short axis slices (heavy white lines) were used for examination of relationship between visual scoring and quantitative measurement. For CMR images, endocardial and epicardial images were outlined in end diastole (ED) and end systole (ES) to obtain wall thickening. Myocardial infarction (hyperenhanced region in middle row image) was manually delineated for measurement of infarct transmurality. Quantitative information was assessed every two degrees and averaged into a 12 segment model per short axis slice (middle). Visual scoring was undertaken using the same 12 segment model (right). For SPECT, a similar approach was used for quantitative measurement (middle) and visual scoring (right) of perfusion.

resolution 50 ms) or a retrospectively vector-ECG-triggered cine steady-state free precession sequence (Philips, spatial resolution $1.25 \times 1.25 \times 8$ mm, gap 2 mm, temporal resolution 33 ms, SENSE factor 2).

Aortic flow was quantified for assessment of aortic or mitral valve regurgitation using a through-plane gradient echo phase contrast (PC) sequence in a transverse plane through the ascending aorta placed at the position of the bifurcation of the pulmonary trunk (Siemens: free breathing, spatial resolution $1.5 \times 1.5 \times 10$ mm, temporal resolution 30 ms, velocity encoding gradient 150 cm/s, prospectively gated with acquisition over 1.3 R-R intervals, Philips: free breathing, spatial resolution $1.2 \times 1.2 \times 10$ mm, temporal resolution 30 ms, velocity encoding gradient 150 cm/s, retrospectively gated).

3.3.2   Image analysis

Global LV parameters

LV EDV, ESV and LVM were determined by manual planimetry of LV endocardial and epicardial contours and Simpsons method in contiguous short-axis cine images using established methods.[185] The end-diastolic time frame was defined as the image acquired immediately following the trigger on the R-wave of the ECG. The end-systolic time frame was determined globally as the time frame where the LV lumen was the smallest. LVM was calculated as the mean of the LVM measured in end-diastolic and end-systolic frames. LVSV was defined as LVEDV−LVESV. LVEF was defined as LVSV/EDV. Volume of infarction was determined by manual planimetry of the hyperenhanced regions in delayed contrast enhancement images. Papillary muscles not contiguous with the myocardial wall in short axis images were excluded from analysis of LVM and infarct volume. IS was defined as infarct volume / LVM volume.

Regional LV function

Visual function scoring of cine CMR images was performed in consensus by two experienced readers blinded to both subject identity and DE CMR images. Function was scored using the 12 segment per slice, four slice model according to the following scale: 0: normal, 1: mild-to-moderate hypokinesis, 2: severe hypokinesis, 3: akinesis, and 4: dyskinesis.

Quantification of function was performed by measurement of wall thickening. Wall thickening was defined as the percent change in radial wall thickness between end diastole and end systole. Endocardial and epicardial borders of the left ventricle were manually delineated in end diastole and end systole, excluding papillary muscles. Wall thickness in end diastole and end systole were quantified

automatically along radial spokes emanating from the centroid of the endocardial delineation (Figure 3.1).

For Paper II and Paper IV, dysfunction in a given segment was defined as wall thickening less than 30%.[186] Paper II sought to analyze the influence of dysfunctional adjacent segments. Figure 3.2 describes the adjacent segment model. An adjacent segment was defined as a myocardial segment that bordered a given segment in the same short axis slice or the same segment in a more basal or apical slice. This resulted in a maximum of four adjacent segments. Hence, the model did not consider segments that were diagonally adjacent in a more basal or apical slice.
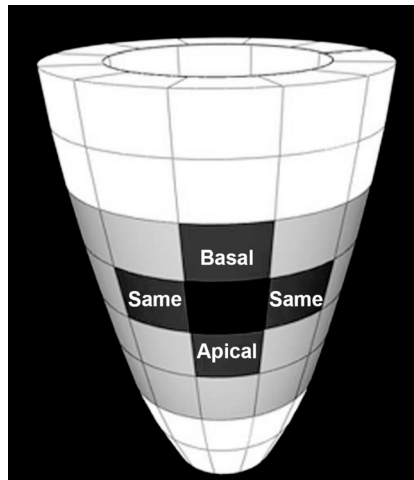

FIGURE 3.2 A schematic diagram of the left ventricle showing the 12 segment per slice model in the four midventricular slices used for analysis (light grey). Four possible adjacent myocardial segments are shown (dark grey) in relation to a given segment (black). An adjacent segment could either be in the same slice (Same), or in a more apical (Apical) or basal (Basal) slice.

Aortic flow and valve regurgitation

Effective SV in the aorta (SV_{Ao}) was determined by manually defining a region of interest (ROI) in the lumen of the ascending aorta in modulus reconstructed PC images. The average signal intensity in the same ROI in the phase reconstructed PC images was multiplied by the velocity encoding gradient and the area of the

region of interest in order to determine instantaneous flow in ml/s at each time point. The sum of all instantaneous flow throughout one cardiac cycle was defined as the SV_{Ao} and effective cardiac output was defined as SV_{Ao} multiplied by the heart rate. The sum of all negative flow was defined as the regurgitant volume through the aortic valve (RV_{Ao}). The sum of all positive flow was defined as the forward volume in the aorta (FV_{Ao}). Regurgitant fraction through the aortic valve (RF_{Ao}) was defined as RV_{Ao}/FV_{Ao}. Regurgitant volume through the mitral valve RV_{mitral} was defined as $LVSV-SV_{Ao}$. Regurgitant fraction through the mitral valve (RF_{mitral}) was defined as $RV_{mitral}/LVSV$.

The upper limit (mean + 2SD) for regurgitant fraction in healthy volunteers has been shown by MRI to be 13% in the mitral valve[187] or 18% in the mitral or aortic valve.[188] Patients were therefore defined as having significant valve regurgitation in either the aortic or mitral valve if the RF_{Ao} or RF_{mitral} exceeded 13%. For the minority of patients where flow quantification was not performed, any mention of visualization of regurgitation from cine CMR images was deemed significant.

3.4   Assessment of viability using DE-MRI

3.4.1   MR imaging

Infarct imaging was performed in late diastole using a segmented inversion recovery turbo fast low-angle shot sequence[71] during breath hold in either 2D or 3D fashion (2D, Siemens: data acquisition every second heart beat, spatial resolution 1.6×1.6×8 mm, gap 2 mm, or 3D, Philips, data acquisition every heart beat, spatial resolution 1.6×1.6×8 mm, gap 0 mm, inversion time set to null normal myocardium). Infarct imaging was typically commenced 10-20 minutes after intravenous injection of 0.2 mmol/kg body weight of an extracellular contrast agent (Gd-DTPA). This approach has been shown to enhance non-viable myocardium[156] due to an increased tissue distribution volume of Gd-DTPA in non-viable regions.[69, 70, 189, 190]

3.4.2   Image analysis

Global infarct size

Volume of infarction was determined by manual planimetry of the hyperenhanced regions in delayed contrast enhancement images. Papillary muscles not contiguous with the myocardial wall in short axis images were excluded from analysis of LVM and infarct volume. Infarct size as percent LVM was defined as infarct volume / LVM volume (%).

Regional infarct transmurality

Manual delineation was undertaken to define the endocardial and epicardial borders of the left ventricle and regions of hyperenhancement in DE CMR images. Quantification of viability was performed by measurement of infarct transmurality. Infarct transmurality was defined as the radial thickness of a region of hyperenhancement expressed as a percent of the total wall thickness in the same position. Infarct thickness and wall thickness were quantified automatically at every other degree along radial spokes emanating from the centroid of the endocardial delineation (Figure 3.1).

3.5 Statistical analyses

Data are presented as mean $\pm$ standard deviation (SD) unless otherwise specified. A p-value of less than 0.05 was considered statistically significant. Variations between normally distributed data were tested by paired t-test and independent t-test as appropriate. Variations between independent data that were not normally distributed were tested by the Mann-Whitney test. Trends were tested by ANOVA with post hoc Bonferroni correction. Wall thickening data is presented graphically as mean $\pm$ SEM to illustrate the physiological trend. Differences between standard deviations were tested by the F-test. Linear regression was determined using Pearson's correlation coefficient.

In Paper II, a linear mixed model assuming compound symmetry (SPSS for Windows, Release 11.0.1) was used to explore the effect size of parameters contributing to wall thickening.

In Paper I, agreement between continuous quantitative measurement and categorical visual scoring of function and perfusion was tested by Kendall's coefficient of concordance (W). Kendall's W varies between 0, denoting no agreement, and 1 denoting maximal agreement. In the absence of accepted criteria for interpretation of the value of Kendall's W, the strength of agreement was interpreted using the same criteria as for interpretation of kappa as adapted by Altman: $<0.20 =$ Poor, 0.21-0.40 $=$ Fair, 0.41-0.60 $=$ Moderate, 0.61-0.80 $=$ Good and 0.81-1.00 $=$ Very good.[191]

In Paper III, the maximum predicted LVEF for patients with IHD was defined as the linear function delimiting the smallest area encompassing 95% of the data for LVEF and IS. The slope and intercept of the linear function were determined from the data using these pre-defined criteria. See Figure 3.3. Line AB was iteratively positioned at the angle Θ and distance CD that would minimize the area of triangle ABC encompassing 95% of the data points.
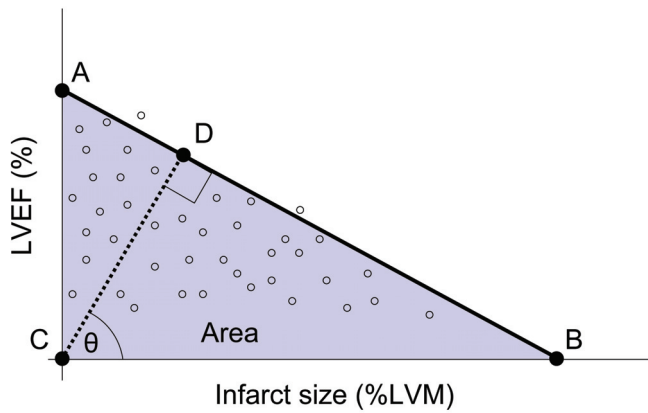
FIGURE 3.3 Schematic diagram of the parameters involved in the iterative process of determining the slope and position of the line describing the maximum predicted LVEF based on infarct size as percent of LVM. Line AB was iteratively positioned at the angle Θ and distance CD that would minimize the area of triangle ABC encompassing 95% of the data points.

Chapter 4

Results and Comments

4.1 Quantitative polar assessment of perfusion, function and viability (Paper I)

Polar plots

The clinical management of patients with IHD involves a complex assessment of the extent and severity of changes in LV myocardial perfusion, function and viability.[192, 193] No previous approaches have undertaken side-by-side presentation of information on perfusion, function and viability as polar plots. Therefore, we sought to develop an integrated method for quantitative polar representation of data from regional myocardial perfusion from SPECT and regional myocardial function and viability from CMR. A population of ten patients with IHD who were scheduled for CABG were studied.

Figure 4.1 shows a representative case illustrating the feasibility of generating polar plots from SPECT and CMR studies of one patient undertaken both before and after three vessel CABG. Myocardium that is hypoperfused and hypofunctioning but viable can easily be identified and localized. Also, improvement in function and perfusion in viable regions after CABG can easily be assessed. See figure text for details. Figure 4.1 demonstrates that quantitative polar representation of LV perfusion, function, and viability is feasible and may provide a method for easy identification of hypofunctioning and hypoperfused but viable myocardium.
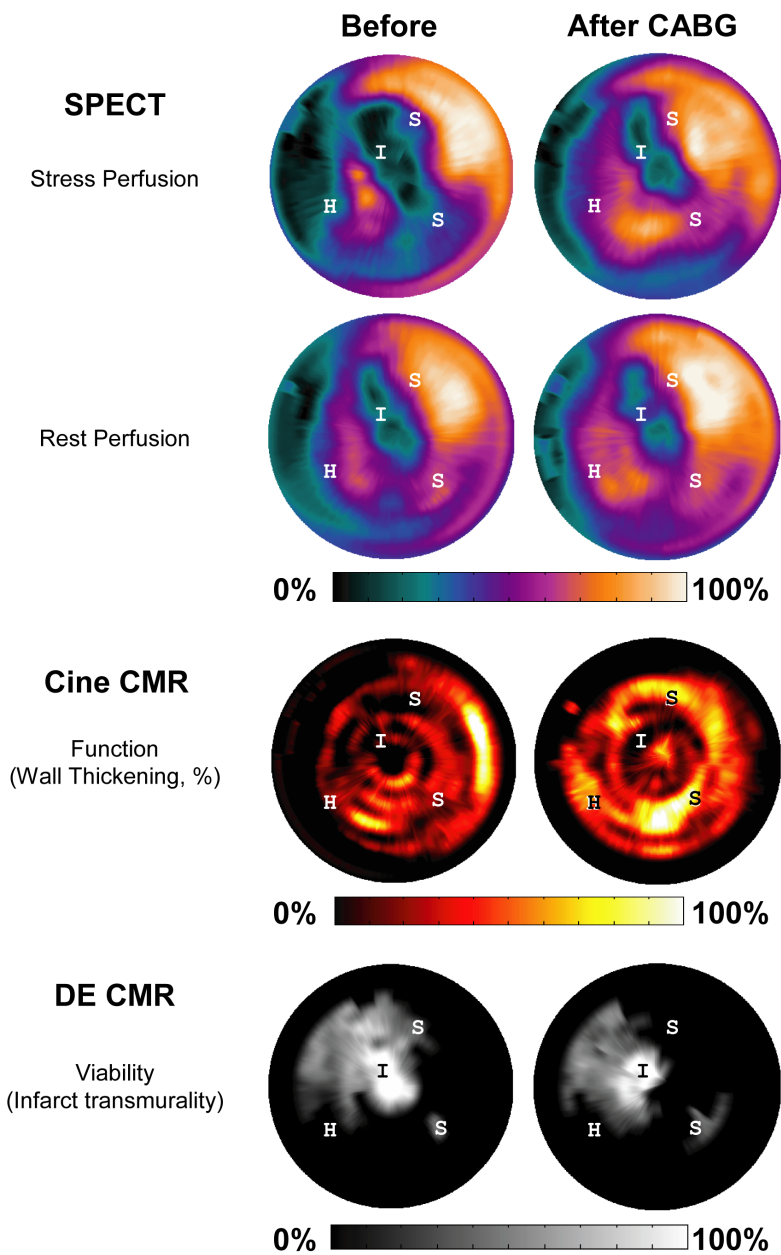
FIGURE 4.1 Example of polar plots generated from rest and stress SPECT perfusion, resting function (wall thickening from cine CMR), and viability (infarct transmurality from DE CMR) in one patient prior to, and one month after CABG. Perfusion is color coded according to a scale where 100% represents the maximum value in the left ventricle. Function is color coded according to a scale representing quantitative wall thickening defined as percent change in wall thickness between diastole and systole. Viability is color coded according to a scale representing quantitative infarct transmurality (%), defined as the percent of the myocardial wall thickness that is hyperenhanced on DE CMR images. "I" indicates a region approaching transmural infarction that exhibits poor function and poor perfusion and does not improve in function after CABG. "H" indicates a region of hibernating myocardium characterized by lack of infarction, poor function and poor perfusion at rest and stress. The hibernating myocardium improves in both rest perfusion, stress perfusion as well as function after CABG. "S" indicates a region of repetitively stunned myocardium characterized by little or no infarction, poor function and reduced stress perfusion. The repetitively stunned myocardium improves in stress perfusion and function after CABG.

Visual scoring and quantitative measurement of perfusion and function

In order to assess the clinical usefulness of the proposed quantitative methods, we also explored the relationship and determined the agreement between visual scoring and quantitative measurement of regional perfusion and function. Figure 4.2 shows the relationship between visual scoring and quantitative measurements of both regional perfusion from SPECT and regional function from cine CMR in 480 myocardial segments from 10 patients. All 480 myocardial segments were assessed with a visual perfusion score. Ten percent of the segments were not assessed with a visual function score due to poor image quality. Kendall's W for testing agreement between quantitative measurement and visual scoring was 1.0 for perfusion and 0.85 for function.

Taken together, the presented findings indicate that quantitative measures of perfusion and function showed a good agreement with visual scoring by experienced observers.
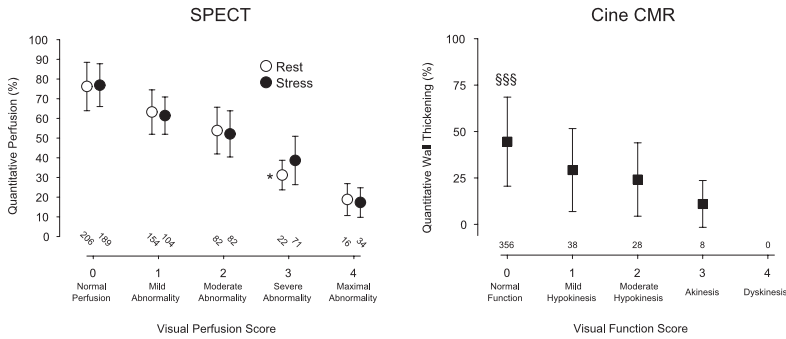
FIGURE 4.2 The relationship between visual scoring and quantitative measurement of perfusion (left) and function (right). The left panel shows data from SPECT at rest (open circles) and stress (filled circles). The right panel shows percent wall thickening and visual function scores from cine CMR at rest. Numbers represent myocardial segments per category. All visual perfusion scores differed significantly in quantitative perfusion ($p < 0.001$ for all except *, denoting $p < 0.05$ for the difference between rest perfusion scores 3 and 4). A normal visual function score differed significantly from all other scores. §§§ denotes $p < 0.001$. Error bars denote SD.

The agreement between quantitative and visual assessment of function was less than for perfusion. The limitations of quantitative echocardiographic methods for identifying visually impaired function have been described.[194] The reason for these limitations, regardless of modality, is unclear. The limitations may be related to the ability of the visual reader to simultaneously assess multiple axes and features of regional function. Examples of such features includes overall atrioventricular plane movement and normalization of thickening to 'normal' segments within the same ventricle. Novel techniques for accurate quantification of multidimensional myocardial strain with high temporal and spatial resolution using CMR have been presented.[74, 195] The future of these research techniques appears to be promising but their roles in the clinical arena have yet to be established.

4.2   Regional wall thickening vs. infarct transmurality (Paper II)

The relationship between regional function and infarct transmurality has been studied by several groups both experimentally[196–198] and clinically.[199–201] We chose to study 20 healthy volunteers and 20 patients assessed after either acute PCI or elective CABG. A duration of six months after revascularization was chosen to minimize the effects of stunning or hibernation on our results. Our findings illustrate that there is a negative and poor correlation between wall thickening and infarct transmurality (R^2=0.11). Figure 4.3 shows wall thickening for controls, and the relationship between wall thickening and quartiles of infarct transmurality for patients with chronic IHD.
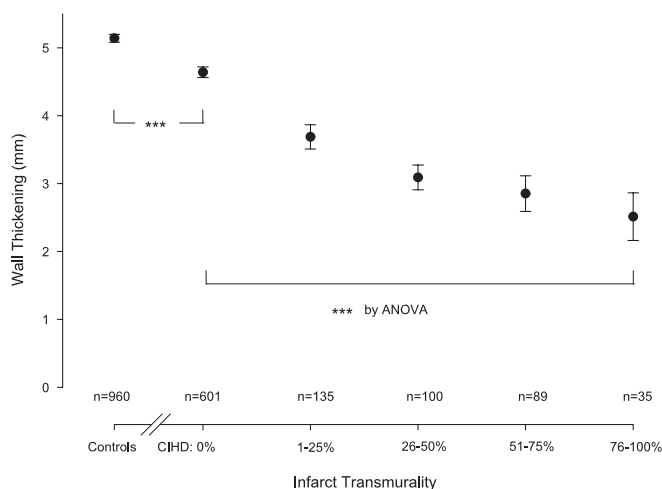

FIGURE 4.3 The relationship between wall thickening and quartiles of infarct transmurality. CIHD denotes patients with chronic ischemic heart disease. Error bars denote SEM. *** denotes p<0.001. n denotes the number of myocardial segments in each group.

These results show a decrease in wall thickening with increasing infarct transmurality. Although it is not shown in Figure 4.3, it is important to note that the standard deviation of the wall thickening for controls and patients with varying

severity of infarct transmurality was close to 2 mm. This implies a considerable variation in the data and overlap between the presented groups. Additional analysis has furthermore shown that quantitative regional myocardial function is influenced more so by the function of adjacent segments and to a lesser extent by infarct transmurality. This is illustrated in Figure 4.4. Thus, wall thickening alone appears to be an inadequate tool for identifying infarction or differentiating between different severities of infarct transmurality. This emphasizes the importance of direct infarct imaging by DE CMR for identifying infarction.
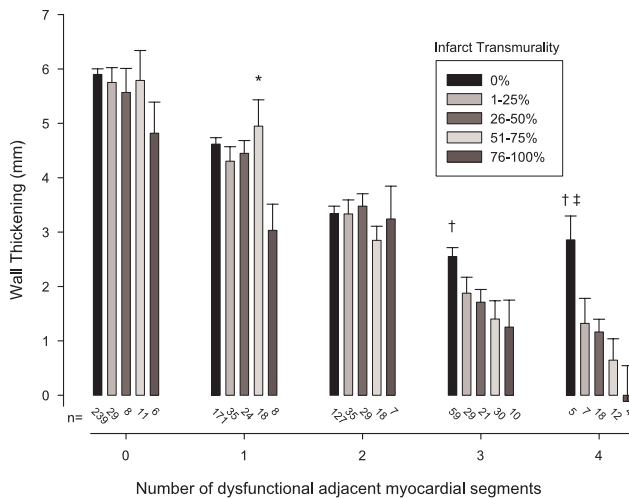

FIGURE 4.4 The relationship between wall thickening and number of dysfunctional adjacent myocardial segments according to infarct transmurality. Note how wall thickening varies more due to the number of dysfunctional adjacent segments than due to infarct transmurality. Error bars denote SEM. * denotes $p<0.05$ vs. 76-100%, † denotes $p<0.01$ vs. 51-75% and ‡ denotes $p<0.01$ vs. 76-100%. Numbers at the bottom of each bar denote the number of myocardial segments in each group.

4.3   LV ejection fraction vs. infarct size (Paper III)

It is important to assess both global function and infarct size when considering revascularization. Previous studies have reported a strong linear correlation be-

tween LVEF and infarct size in selected populations.[202–204] However, this relationship has been shown to have a weaker correlation in larger and more heterogeneous patient populations studied with nuclear techniques, possibly due to the influence of ischemia.[205,206] We chose to retrospectively study 156 consecutive patients with IHD who were clinically referred for viability assessment using DE CMR at our institution. Figure 4.5 illustrates the relationship between LVEF and infarct size assessed by CMR. By comparison, Figure 4.6 illustrates the relationship between EDV, ESV, SV and infarct size. The correlation between LVEF and infarct size was $R^2=0.25$ and it appears that LVEF is superior to EDV ($R^2=0.12$), ESV ($R^2=0.15$) and SV ($R^2=0.05$) when it comes to assessing the relationship between global LV function and IS.
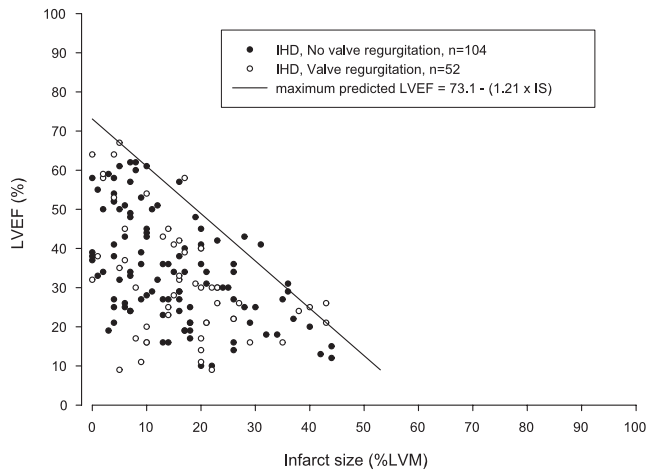

FIGURE 4.5 The relationship between LVEF and infarct size (%LVM) for patients with IHD and the absence (black circles) or presence (open circles) of significant regurgitation in the aortic or mitral valve. The solid line represents the maximum predicted LVEF for a given IS determined using data from all patients with IHD as described in Figure 3.3. Patients with or without significant valve regurgitation did not differ from each other with regards to either LVEF or infarct size.

The presented relationship between LVEF and infarct size as assessed by CMR illustrates the difficulty of accurately assessing infarct size based on LVEF alone. This further underscores the importance of direct infarct imaging with CMR for
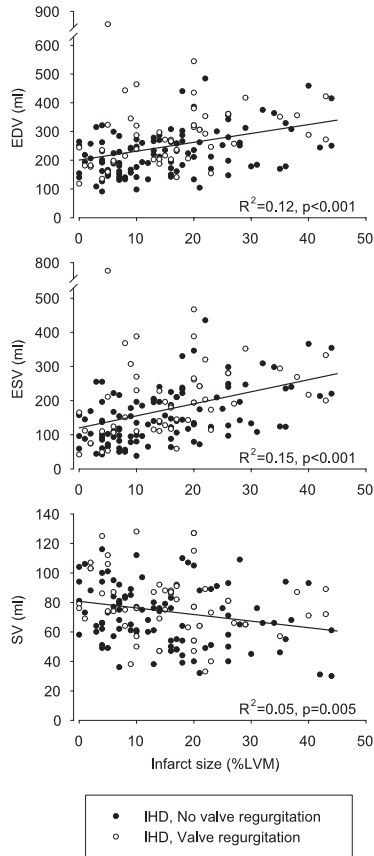
FIGURE 4.6 The relationship between EDV (top), ESV (middle), SV (bottom) and IS (%LVM) for patients with IHD and the absence (black circles) or presence (open circles) of significant regurgitation in the aortic or mitral valve. The solid lines represent linear regression using data from all data points.

accurate assessment of infarct size. Moreover, the presented maximum predicted LVEF in relation to infarct size offers the possibility of assessing the potential for a patient to improve from a given LVEF to the maximum predicted LVEF for a given infarct size. Future studies are warranted to assess the clinical utility of such an assessment.

4.4 Recovery of LV function and perfusion in relation to infarction (Paper IV)

Paper IV consisted of a study population of 15 patients scheduled for first time elective revascularization by CABG or PCI. They were imaged by SPECT and MRI before and both one and six months following revascularization. The distribution of segmental infarct transmurality for these patients indicates that the infarctions in the population were primarily <50% transmural.

Figure 4.7 shows the time course of quantitative regional wall thickening and perfusion for both segments with and without dysfunction prior to revascularization. These results show that dysfunctional segments without infarction gained the greatest improvement in both perfusion and function within one month after revascularization. In contrast, segments with infarction, which was predominantly <50% transmural in our population, showed delayed functional recovery at six months despite improvements in perfusion at one month. Mean LVEF in the population did not change at either one or six months after surgery. Surprisingly, segments without baseline dysfunction showed a reduction in wall thickening at one month regardless of presence of infarction. Our findings of simultaneous improvement and deterioration of regional function in segments of different baseline functional status can be better understood when considering the lack of change in LVEF in our population.

Previous studies using echocardiography and scintigraphic techniques have demonstrated that the time course of regional functional recovery following CABG begins immediately following revascularization and may continue up to between three and 14 months after surgery.[31,37,207–211] For example, Bax *et al*[211] showed no functional improvement in segments with either non-transmural or transmural infarction as determined by [18]FDG uptake using SPECT. Yet, segments with reduced perfusion but no sign of infarct using [18]FDG improved function both three and 14 months after revascularization.

The discrepancy in the time course of functional recovery between previous results and ours may be due to the limited spatial resolution of SPECT for defining the presence and transmurality of infarction. Furthermore, late improvements in function assessed visually by echocardiography have been associated with preoperative histological and scintigraphic measures of ischemic burden.[31,37,208–211]
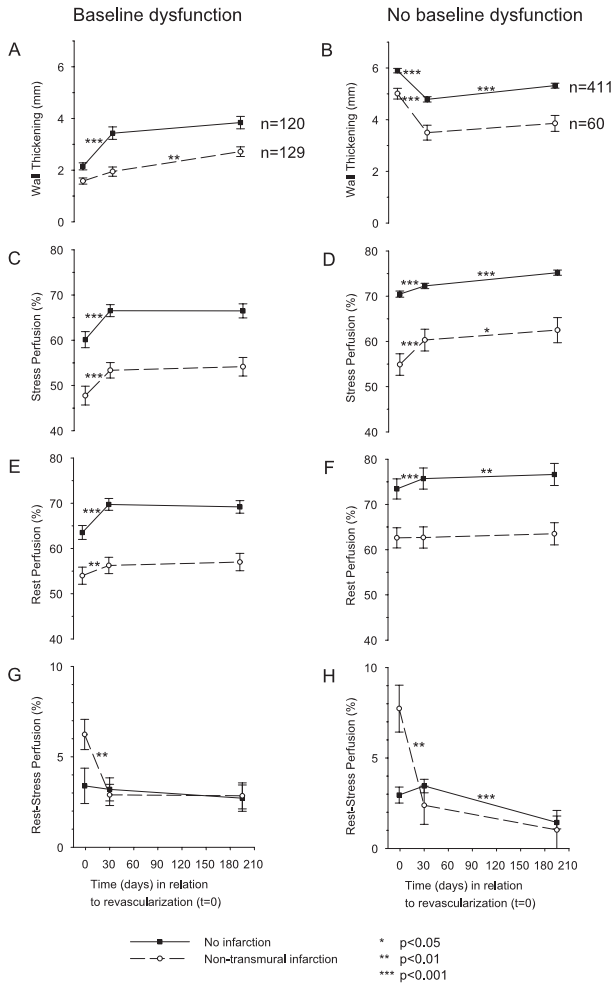
FIGURE 4.7 Time course of regional function and perfusion after revascularization according to presence (left) or absence (right) of dysfunction prior to revascularization. Quantitative wall thickening (A, B) was assessed by cine MRI. Stress perfusion (C, D) and rest perfusion (E, F) were assessed by ^{99m}Tc-tetrofosmin SPECT. Reversible perfusion is presented as the difference between rest and stress perfusion (G, H). Black squares and open circles denote myocardial segments without and with infarction, respectively, as assessed by delayed enhancement MRI. Error bars represent SEM.

Such histological measures of ischemic burden have been shown to independently correlate to both scintigraphic findings[32, 212–214] and an increased duration of ischemia resulting in a delayed functional recovery.[36] Therefore, one potential explanation for our findings of the difference in time course of functional recovery between segments with and without infarction may be a more severe degree of ischemic burden in the viable portion of the segments with infarction. This is supported by our finding of a greater initial difference in rest-stress perfusion in these segments.

Chapter 5

Conclusions

This thesis illustrates the necessity to perform quantitative assessment of function, perfusion and viability in combination when studying the pathophysiology of dysfunctional but viable myocardium in IHD.

The presented studies emphasize the importance of direct infarct imaging by CMR for the accurate identification of infarction in the assessment of dysfunctional myocardium. Neither regional nor global myocardial function have a close correlation to infarction, but the presence of non-transmural infarction is a marker for delayed recovery of function following revascularization.

The major conclusions for each paper were:

  I. Integrated polar representation of function, perfusion and viability is feasible, and the proposed quantitative methods show good agreement with visual assessment for perfusion from SPECT and function from CMR.

  II. Regional function decreases with increasing infarct transmurality. However, the variation in regional function is large, and importantly, influenced more so by the function of adjacent myocardium than by infarct transmurality.

  III. LVEF cannot be used to estimate infarct size, and vice versa. However, LVEF can be used to estimate a maximum predicted infarct size, and infarct size can be used to estimate a maximum predicted LVEF.

  IV. The recovery of perfusion after revascularization occurs in the first month, while the recovery of function is delayed in regions with non-transmural myocardial infarction, possibly due to a more severe initial ischemic burden.

Acknowledgments

I would like to thank the people who have contributed in one way or another to this thesis.

My supervisor, **Håkan Arheden**, for your untethered openness, friendship, patience, enthusiasm, clarity of thought and communication, and for believing in me. For providing and continuing to build a research environment with such wonderful coworkers.

Co-supervisor, **Peter Cain**, for friendship and stamina in teaching me the ways of science and guidance through challenging times.

John Palmer, for putting up with my questions, teaching me SPECT and providing outstanding support and realistic optimism in our collaboration.

Björn Jonson, for fostering a clinical research department which is open to so many inspiring colleagues.

Olle Pahlm, for valuable scientific discussions and humble linguistic support.

Marcus Carlsson, **Erik Hedström**, **Henrik Engblom**, **Erik Bergvall**, **Karin Markenroth** and **Einar Heiberg** for making cardiac MRI so much fun and for being great friends and colleagues.

Co-authors **Björn Ekmehag**, **Pelle Johnsson** and **Annick Perron**, for fruitful collaboration.

Freddy Ståhlberg, for introducing me to MR physics with unbridled enthusiasm and for valuable comments on the MR theory in this thesis.

Galen S. Wagner, for stimulating discussions and inspiration early in my research training.

Doctors, nurses, technicians, physicists, technical staff and administrative staff at the Departments of **Clinical Physiology**, **Radiology**, **Thoracic Surgery** and **Cardiology** at Lund University Hospital, for such an optimistic, understanding and flexible attitude, without which the studies in this thesis would have been far more difficult to undertake.

My parents **Margareta** and **Mikael**, for being excellent parents and for stimulating my curiosity from an early age.

My brothers, **Olof** and **Johan**, for friendship and for being cool brothers.

Finally, **Lena**, for unconditional love, endless optimism, home front support and understanding.

Bibliography

[1] Remme WJ, Swedberg K. Guidelines for the diagnosis and treatment of chronic heart failure. *Eur Heart J*, 22(17):1527–60, 2001.

[2] Heart disease and stroke statistics, 2005 update. *American Heart Association*, 2005.

[3] Gheorghiade M, Bonow RO. Chronic heart failure in the United States: a manifestation of coronary artery disease. *Circulation*, 97(3):282–9, 1998.

[4] Boersma E, Doornbos G, Bloemberg B. *Cardiovascular diseases in Europe. European registries of cardiovascular diseases and patient management.* Sophia Antipolis, France, 1999.

[5] Yusuf S, Reddy S, Ounpuu S, Anand S. Global burden of cardiovascular diseases: part I: general considerations, the epidemiologic transition, risk factors, and impact of urbanization. *Circulation*, 104(22):2746–53, 2001.

[6] Nesto RW, Kowalchuk GJ. The ischemic cascade: temporal sequence of hemodynamic, electrocardiographic and symptomatic expressions of ischemia. *Am J Cardiol*, 59(7):23C–30C, 1987.

[7] Rizzello V, Poldermans D, Bax JJ. Assessment of myocardial viability in chronic ischemic heart disease: current status. *Q J Nucl Med Mol Imaging*, 49(1):81–96, 2005.

[8] Underwood SR, Anagnostopoulos C, Cerqueira M, Ell PJ, Flint EJ, Harbinson M, Kelion AD, Al-Mohammad A, Prvulovich EM, et al. Myocardial perfusion scintigraphy: the evidence. *Eur J Nucl Med Mol Imaging*, 31(2):261–91, 2004.

[9] Naghavi M, Libby P, Falk E, Casscells SW, Litovsky S, Rumberger J, Badimon JJ, Stefanadis C, Moreno P, et al. From vulnerable plaque to vulnerable patient: a call for new definitions and risk assessment strategies: Part I. *Circulation*, 108(14):1664–72, 2003.

[10] Opie LH. *The Heart, Physiology, from Cell to Circulation*. Lippincott-Raven, Philadelphia, 1998.

[11] Korge P, Byrd SK, Campbell KB. Functional coupling between sarcoplasmic-reticulum-bound creatine kinase and Ca(2+)-ATPase. *Eur J Biochem*, 213(3):973–80, 1993.

[12] Cross HR, Clarke K, Opie LH, Radda GK. Is lactate-induced myocardial ischaemic injury mediated by decreased pH or increased intracellular lactate? *J Mol Cell Cardiol*, 27(7):1369–81, 1995.

[13] Eisner DA, Smith TW. The Na-K pump and its effectors in cardiac muscle. In FH A, editor, *The Heart and Cardiovascular System. 2nd ed.* Raven Press, New York, 1992.

[14] Sylven C. Mechanisms of pain in angina pectoris–a critical review of the adenosine hypothesis. *Cardiovasc Drugs Ther*, 7(5):745–59, 1993.

[15] Reimer KA, Jennings RB. The "wavefront phenomenon" of myocardial ischemic cell death. II. Transmural progression of necrosis within the framework of ischemic bed size (myocardium at risk) and collateral flow. *Lab Invest*, 40(6):633–44, 1979.

[16] Heusch G, Schulz R, Rahimtoola SH. Myocardial hibernation: a delicate balance. *Am J Physiol Heart Circ Physiol*, 288(3):H984–99, 2005.

[17] Ardehali A, Ports TA. Myocardial oxygen supply and demand. *Chest*, 98(3):699–705, 1990.

[18] Hachamovitch R, Berman DS, Shaw LJ, Kiat H, Cohen I, Cabico JA, Friedman J, Diamond GA. Incremental prognostic value of myocardial perfusion single photon emission computed tomography for the prediction of cardiac death: differential stratification for risk of cardiac death and myocardial infarction. *Circulation*, 97(6):535–43, 1998.

[19] Braunwald E, Kloner RA. The stunned myocardium: prolonged, postischemic ventricular dysfunction. *Circulation*, 66(6):1146–9, 1982.

[20] Heyndrickx GR, Millard RW, McRitchie RJ, Maroko PR, Vatner SF. Regional myocardial functional and electrophysiological alterations after brief coronary artery occlusion in conscious dogs. *J Clin Invest*, 56(4):978–85, 1975.

[21] Lavallee M, Cox D, Patrick TA, Vatner SF. Salvage of myocardial function by coronary artery reperfusion 1, 2, and 3 hours after occlusion in conscious dogs. *Circ Res*, 53(2):235–47, 1983.

[22] Bush LR, Buja LM, Samowitz W, Rude RE, Wathen M, Tilton GD, Willerson JT. Recovery of left ventricular segmental function after long-term reperfusion following temporary coronary occlusion in conscious dogs. Comparison of 2- and 4-hour occlusions. *Circ Res*, 53(2):248–63, 1983.

[23] Bolli R. Mechanism of myocardial "stunning". *Circulation*, 82(3):723–38, 1990.

[24] Moens AL, Claeys MJ, Timmermans JP, Vrints CJ. Myocardial ischemia/reperfusion-injury, a clinical view on a complex pathophysiological process. *Int J Cardiol*, 100(2):179–90, 2005.

[25] Homans DC, Sublett E, Dai XZ, Bache RJ. Persistence of regional left ventricular dysfunction after exercise-induced myocardial ischemia. *J Clin Invest*, 77(1):66–73, 1986.

[26] Ambrosio G, Betocchi S, Pace L, Losi MA, Perrone-Filardi P, Soricelli A, Piscione F, Taube J, Squame F, et al. Prolonged impairment of regional contractile function after resolution of exercise-induced angina. Evidence of myocardial stunning in patients with coronary artery disease. *Circulation*, 94(10):2455–64, 1996.

[27] Nicklas JM, Becker LC, Bulkley BH. Effects of repeated brief coronary occlusion on regional left ventricular function and dimension in dogs. *Am J Cardiol*, 56(7):473–8, 1985.

[28] Homans DC, Laxson DD, Sublett E, Lindstrom P, Bache RJ. Cumulative deterioration of myocardial function after repeated episodes of exercise-induced ischemia. *Am J Physiol*, 256(5 Pt 2):H1462–71, 1989.

[29] Rahimtoola SH. The hibernating myocardium. *Am Heart J*, 117(1):211–21, 1989.

[30] Nienaber CA, Brunken RC, Sherman CT, Yeatman LA, Gambhir SS, Krivokapich J, Demer LL, Ratib O, Child JS, et al. Metabolic and functional recovery of ischemic human myocardium after coronary angioplasty. *J Am Coll Cardiol*, 18(4):966–78, 1991.

[31] Takeishi Y, Tono-oka I, Kubota I, Ikeda K, Masakane I, Chiba J, Abe S, Tsuiki K, Komatani A, et al. Functional recovery of hibernating myocardium after coronary bypass surgery: does it coincide with improvement in perfusion? *Am Heart J*, 122(3 Pt 1):665–70, 1991.

[32] Maes A, Flameng W, Borgers M, Nuyts J, Ausma J, Bormans G, Van de Werf F, De Roo M, Mortelmans L. Regional myocardial blood flow, glucose utilization and contractile function before and after revascularization and ultrastructural findings in patients with chronic coronary artery disease. *Eur J Nucl Med*, 22(11):1299–305, 1995.

[33] Altehoefer C, vom Dahl J, Messmer BJ, Hanrath P, Buell U. Fate of the resting perfusion defect as assessed with technetium-99m methoxy-isobutyl-isonitrile single-photon emission computed tomography after successful revascularization in patients with healed myocardial infarction. *Am J Cardiol*, 77(1):88–92, 1996.

[34] Paluszkiewicz L, Kwinecki P, Jemielity M, Szyszka A, Dyszkiewicz W, Cieslinski A. Myocardial perfusion correlates with improvement of systolic function of the left ventricle after CABG. Dobutamine echocardiography and Tc-99m-MIBI SPECT study. *Eur J Cardiothorac Surg*, 21(1):32–5, 2002.

[35] Ugander M, Cain P, Johnsson P, Palmer J, Arheden H. Influence of the presence of chronic non-transmural myocardial infarction on the time course of perfusion and functional recovery after revascularization. *Manuscript, appended Paper IV*.

[36] Schwarz ER, Schoendube FA, Kostin S, Schmiedtke N, Schulz G, Buell U, Messmer BJ, Morrison J, Hanrath P, vom Dahl J. Prolonged myocardial hibernation exacerbates cardiomyocyte degeneration and impairs recovery of function after revascularization. *J Am Coll Cardiol*, 31(5):1018–26, 1998.

[37] Vanoverschelde JL, Depre C, Gerber BL, Borgers M, Wijns W, Robert A, Dion R, Melin JA. Time course of functional recovery after coronary artery bypass graft surgery in patients with chronic left ventricular ischemic dysfunction. *Am J Cardiol*, 85(12):1432–9, 2000.

[38] Schwarz ER, Schaper J, vom Dahl J, Altehoefer C, Grohmann B, Schoendube F, Sheehan FH, Uebis R, Buell U, et al. Myocyte degeneration and cell death in hibernating human myocardium. *J Am Coll Cardiol*, 27(7):1577–85, 1996.

[39] Hughes GC, Landolfo CK, Yin B, DeGrado TR, Coleman RE, Landolfo KP, Lowe JE. Is chronically dysfunctional yet viable myocardium distal to a severe coronary stenosis hypoperfused? *Ann Thorac Surg*, 72(1):163–8, 2001.

[40] Marinho NV, Keogh BE, Costa DC, Lammerstma AA, Ell PJ, Camici PG. Pathophysiology of chronic left ventricular dysfunction. New insights from the measurement of absolute myocardial blood flow and glucose utilization. *Circulation*, 93(4):737–44, 1996.

[41] Hernandez-Pampaloni M, Bax JJ, Morita K, Dutka DP, Camici PG. Incidence of stunned, hibernating and scarred myocardium in ischaemic cardiomyopathy. *Eur J Nucl Med Mol Imaging*, 32(3):314–21, 2005.

[42] Auerbach MA, Schoder H, Hoh C, Gambhir SS, Yaghoubi S, Sayre JW, Silverman D, Phelps ME, Schelbert HR, Czernin J. Prevalence of myocardial viability as detected by positron emission tomography in patients with ischemic cardiomyopathy. *Circulation*, 99(22):2921–6, 1999.

[43] al Mohammad A, Mahy IR, Norton MY, Hillis G, Patel JC, Mikecz P, Walton S. Prevalence of hibernating myocardium in patients with severely impaired ischaemic left ventricles. *Heart*, 80(6):559–64, 1998.

[44] Bonow RO. Identification of viable myocardium. *Circulation*, 94(11):2674–80, 1996.

[45] Allman KC, Shaw LJ, Hachamovitch R, Udelson JE. Myocardial viability testing and impact of revascularization on prognosis in patients with coronary artery disease and left ventricular dysfunction: a meta-analysis. *J Am Coll Cardiol*, 39(7):1151–8, 2002.

[46] Emond M, Mock MB, Davis KB, Fisher LD, Holmes D R J, Chaitman BR, Kaiser GC, Alderman E, Killip T. Long-term survival of medically treated patients in the Coronary Artery Surgery Study (CASS) Registry. *Circulation*, 90(6):2645–57, 1994.

[47] Togni M, Balmer F, Pfiffner D, Maier W, Zeiher AM, Meier B. Percutaneous coronary interventions in Europe 1992-2001. *Eur Heart J*, 25(14):1208–13, 2004.

[48] Packer M, Bristow MR, Cohn JN, Colucci WS, Fowler MB, Gilbert EM, Shusterman NH. The effect of carvedilol on morbidity and mortality in patients with chronic heart failure. U.S. Carvedilol Heart Failure Study Group. *N Engl J Med*, 334(21):1349–55, 1996.

[49] Braunwald E. Expanding indications for beta-blockers in heart failure. *N Engl J Med*, 344(22):1711–2, 2001.

[50] Pitt B, Segal R, Martinez FA, Meurers G, Cowley AJ, Thomas I, Deedwania PC, Ney DE, Snavely DB, Chang PI. Randomised trial of losartan versus captopril in patients over 65 with heart failure (Evaluation of Losartan in the Elderly Study, ELITE). *Lancet*, 349(9054):747–52, 1997.

[51] Cairns JA, Connolly SJ, Roberts R, Gent M. Randomised trial of outcome after myocardial infarction in patients with frequent or repetitive ventricular premature depolarisations: CAMIAT. Canadian Amiodarone Myocardial Infarction Arrhythmia Trial Investigators. *Lancet*, 349(9053):675–82, 1997.

[52] Cowie MR, Wood DA, Coats AJ, Thompson SG, Poole-Wilson PA, Suresh V, Sutton GC. Incidence and aetiology of heart failure; a population-based study. *Eur Heart J*, 20(6):421–8, 1999.

[53] Baker DW, Jones R, Hodges J, Massie BM, Konstam MA, Rose EA. Management of heart failure. III. The role of revascularization in the treatment of patients with moderate or severe left ventricular systolic dysfunction. *Jama*, 272(19):1528–34, 1994.

[54] Pigott JD, Kouchoukos NT, Oberman A, Cutter GR. Late results of surgical and medical therapy for patients with coronary artery disease and depressed left ventricular function. *J Am Coll Cardiol*, 5(5):1036–45, 1985.

[55] Bom N, Ligtvoet CM. Principles of cardiac ultrasound. In JRTC Roelandt, GR Sutherland, S Iliceto, D Linker, editors, *Cardiac Ultrasound*. Churchill Livingstone, 1993.

[56] Lepper W, Belcik T, Wei K, Lindner JR, Sklenar J, Kaul S. Myocardial contrast echocardiography. *Circulation*, 109(25):3132–5, 2004.

[57] Jansson K, Fransson SG. Mortality related to coronary angiography. *Clin Radiol*, 51(12):858–60, 1996.

[58] Ohnesorge BM, Becker CR, Flohr TG, Reiser MF. *Multi-slice CT in Cardiac Imaging*. Springer-Verlag, 2002.

[59] Raff GL, Gallagher MJ, O'Neill WW, Goldstein JA. Diagnostic accuracy of noninvasive coronary angiography using 64-slice spiral computed tomography. *J Am Coll Cardiol*, 46(3):552–7, 2005.

[60] Germano G, Berman DS. *Clinical Gated Cardiac SPECT*. Futura Publishing Company, Armonk, New York, 1999.

[61] Dilsizian V, Perrone-Filardi P, Arrighi JA, Bacharach SL, Quyyumi AA, Freedman NM, Bonow RO. Concordance and discordance between stress-redistribution-reinjection and rest-redistribution thallium imaging for assessing viable myocardium. Comparison with metabolic activity by positron emission tomography. *Circulation*, 88(3):941–52, 1993.

[62] Smith WH, Kastner RJ, Calnon DA, Segalla D, Beller GA, Watson DD. Quantitative gated single photon emission computed tomography imaging: a counts-based method for display and measurement of regional and global ventricular systolic function. *J Nucl Cardiol*, 4(6):451–63, 1997.

[63] Hassan N, Escanye JM, Juilliere Y, Marie PY, David N, Olivier P, Ayalew A, Karcher G, Stolz JF, Bertrand A. 201Tl SPECT abnormalities, documented at rest in dilated cardiomyopathy, are related to a lower than normal myocardial thickness but not to an excess in myocardial wall stress. *J Nucl Med*, 43(4):451–7, 2002.

[64] Masood Y, Liu Y, DePuey G. Clinical validation of attenuation correction using x-ray CT-derived attenuation maps. Multicenter clinical trial with angiographic correlation. *J Nucl Cardiol*, page (in press), 2005.

[65] Larson AC, White RD, Laub G, McVeigh ER, Li D, Simonetti OP. Self-gated cardiac cine MRI. *Magn Reson Med*, 51(1):93–102, 2004.

[66] Crowe ME, Larson AC, Zhang Q, Carr J, White RD, Li D, Simonetti OP. Automated rectilinear self-gated cardiac cine imaging. *Magn Reson Med*, 52(4):782–8, 2004.

[67] Larson AC, Kellman P, Arai A, Hirsch GA, McVeigh E, Li D, Simonetti OP. Preliminary investigation of respiratory self-gating for free-breathing segmented cine MRI. *Magn Reson Med*, 53(1):159–68, 2005.

[68] Tsao J, Boesiger P, Pruessmann KP. k-t BLAST and k-t SENSE: dynamic MRI with high frame rate exploiting spatiotemporal correlations. *Magn Reson Med*, 50(5):1031–42, 2003.

[69] Arheden H, Saeed M, Higgins CB, Gao DW, Bremerich J, Wyttenbach R, Dae MW, Wendland MF. Measurement of the distribution volume of gadopentetate dimeglumine at echo-planar MR imaging to quantify myocardial infarction: comparison with 99mTc-DTPA autoradiography in rats. *Radiology*, 211(3):698–708, 1999.

[70] Klein C, Nekolla SG, Balbach T, Schnackenburg B, Nagel E, Fleck E, Schwaiger M. The influence of myocardial blood flow and volume of distribution on late Gd-DTPA kinetics in ischemic heart failure. *J Magn Reson Imaging*, 20(4):588–93, 2004.

[71] Simonetti OP, Kim RJ, Fieno DS, Hillenbrand HB, Wu E, Bundy JM, Finn JP, Judd RM. An improved MR imaging technique for the visualization of myocardial infarction. *Radiology*, 218(1):215–23, 2001.

[72] Abdel-Aty H, Zagrosek A, Schulz-Menger J, Taylor AJ, Messroghli D, Kumar A, Gross M, Dietz R, Friedrich MG. Delayed enhancement and T2-weighted cardiovascular magnetic resonance imaging differentiate acute from chronic myocardial infarction. *Circulation*, 109(20):2411–6, 2004.

[73] Schulz-Menger J, Gross M, Messroghli D, Uhlich F, Dietz R, Friedrich MG. Cardiovascular magnetic resonance of acute myocardial infarction at a very early stage. *J Am Coll Cardiol*, 42(3):513–8, 2003.

[74] Bergvall E, Cain P, Sparr G, Arheden H. Very Fast and Highly Automated Approach to Myocardial Motion Analysis Using Phase Contrast MRI (poster abstract). *Journal of Cardiovascular Magnetic Resonance*, 6(1):394–395, 2004.

[75] Kim WY, Danias PG, Stuber M, Flamm SD, Plein S, Nagel E, Langerak SE, Weber OM, Pedersen EM, et al. Coronary magnetic resonance angiography for the detection of coronary stenoses. *N Engl J Med*, 345(26):1863–9, 2001.

[76] Kim WY, Stuber M, Bornert P, Kissinger KV, Manning WJ, Botnar RM. Three-dimensional black-blood cardiac magnetic resonance coronary vessel wall imaging detects positive arterial remodeling in patients with nonsignificant coronary artery disease. *Circulation*, 106(3):296–9, 2002.

[77] Francis JM, Pennell DJ. Treatment of claustrophobia for cardiovascular magnetic resonance: use and effectiveness of mild sedation. *J Cardiovasc Magn Reson*, 2(2):139–41, 2000.

[78] Pennell DJ, Sechtem UP, Higgins CB, Manning WJ, Pohost GM, Rademakers FE, van Rossum AC, Shaw LJ, Yucel EK. Clinical indications for cardiovascular magnetic resonance (CMR): Consensus Panel report. *J Cardiovasc Magn Reson*, 6(4):727–65, 2004.

[79] Longmore DB, Klipstein RH, Underwood SR, Firmin DN, Hounsfield GN, Watanabe M, Bland C, Fox K, Poole-Wilson PA, et al. Dimensional accuracy of magnetic resonance in studies of the heart. *Lancet*, 1(8442):1360–2, 1985.

[80] Rehr RB, Malloy CR, Filipchuk NG, Peshock RM. Left ventricular volumes measured by MR imaging. *Radiology*, 156(3):717–9, 1985.

[81] Semelka RC, Tomei E, Wagner S, Mayo J, Caputo G, O'Sullivan M, Parmley WW, Chatterjee K, Wolfe C, Higgins CB. Interstudy reproducibility of dimensional and functional measurements between cine magnetic resonance studies in the morphologically abnormal left ventricle. *Am Heart J*, 119(6):1367–73, 1990.

[82] Semelka RC, Tomei E, Wagner S, Mayo J, Kondo C, Suzuki J, Caputo GR, Higgins CB. Normal left ventricular dimensions and function: interstudy reproducibility of measurements with cine MR imaging. *Radiology*, 174(3 Pt 1):763–8, 1990.

[83] Mogelvang J, Lindvig K, Sondergaard L, Saunamaki K, Henriksen O. Reproducibility of cardiac volume measurements including left ventricular mass determined by MRI. *Clin Physiol*, 13(6):587–97, 1993.

[84] Bellenger NG, Davies LC, Francis JM, Coats AJ, Pennell DJ. Reduction in sample size for studies of remodeling in heart failure by the use of cardiovascular magnetic resonance. *J Cardiovasc Magn Reson*, 2(4):271–8, 2000.

[85] Grothues F, Smith GC, Moon JC, Bellenger NG, Collins P, Klein HU, Pennell DJ. Comparison of interstudy reproducibility of cardiovascular magnetic resonance with two-dimensional echocardiography in normal subjects and in patients with heart failure or left ventricular hypertrophy. *Am J Cardiol*, 90(1):29–34, 2002.

[86] Gutierrez-Chico JL, Zamorano JL, Perez de Isla L, Orejas M, Almeria C, Rodrigo JL, Ferreiros J, Serra V, Macaya C. Comparison of left ventricular volumes and ejection fractions measured by three-dimensional echocardiography versus by two-dimensional echocardiography and cardiac magnetic resonance in patients with various cardiomyopathies. *Am J Cardiol*, 95(6):809–13, 2005.

[87] Tadamura E, Kudoh T, Motooka M, Inubushi M, Shirakawa S, Hattori N, Okada T, Matsuda T, Koshiji T, et al. Assessment of regional and global left ventricular function by reinjection T1-201 and rest Tc-99m sestamibi ECG-gated SPECT: comparison with three-dimensional magnetic resonance imaging. *J Am Coll Cardiol*, 33(4):991–7, 1999.

[88] Tadamura E, Kudoh T, Motooka M, Inubushi M, Okada T, Kubo S, Hattori N, Matsuda T, Koshiji T, et al. Use of technetium-99m sestamibi ECG-gated single-photon emission tomography for the evaluation of left ventricular function following coronary artery bypass graft: comparison with three-dimensional magnetic resonance imaging. *Eur J Nucl Med*, 26(7):705–12, 1999.

[89] Vaduganathan P, He ZX, Vick GW, Mahmarian JJ, Verani MS. Evaluation of left ventricular wall motion, volumes, and ejection fraction by gated myocardial tomography with technetium 99m-labeled tetrofosmin: a comparison with cine magnetic resonance imaging. *J Nucl Cardiol*, 6(1 Pt 1):3–10, 1999.

[90] Bavelaar-Croon CD, Kayser HW, van der Wall EE, de Roos A, Dibbets-Schneider P, Pauwels EK, Germano G, Atsma DE. Left ventricular function: correlation of quantitative gated SPECT and MR imaging over a wide range of values. *Radiology*, 217(2):572–5, 2000.

[91] Bax JJ, Lamb H, Dibbets P, Pelikan H, Boersma E, Viergever EP, Germano G, Vliegen HW, de Roos A, et al. Comparison of gated single-photon emission computed tomography with magnetic resonance imaging for evaluation of left ventricular function in ischemic cardiomyopathy. *Am J Cardiol*, 86(12):1299–305, 2000.

[92] Faber TL, Vansant JP, Pettigrew RI, Galt JR, Blais M, Chatzimavroudis G, Cooke CD, Folks RD, Waldrop SM, et al. Evaluation of left ventricular endocardial volumes and ejection fractions computed from gated perfusion SPECT with magnetic resonance imaging: comparison of two methods. *J Nucl Cardiol*, 8(6):645–51, 2001.

[93] Thorley PJ, Plein S, Bloomer TN, Ridgway JP, Sivananthan UM. Comparison of 99mTc tetrofosmin gated SPECT measurements of left ventricular volumes and ejection fraction with MRI over a wide range of values. *Nucl Med Commun*, 24(7):763–9, 2003.

[94]   Lipke CS, Kuhl HP, Nowak B, Kaiser HJ, Reinartz P, Koch KC, Buell U, Schaefer WM. Validation of 4D-MSPECT and QGS for quantification of left ventricular volumes and ejection fraction from gated 99mTc-MIBI SPET: comparison with cardiac magnetic resonance imaging. *Eur J Nucl Med Mol Imaging*, 31(4):482–90, 2004.

[95]   Persson E, Carlsson M, Palmer J, Pahlm O, Arheden H. Evaluation of left ventricular volumes and ejection fraction by automated gated myocardial SPECT versus cardiovascular magnetic resonance. *Clin Physiol Funct Imaging*, 25(3):135–41, 2005.

[96]   Yamamuro M, Tadamura E, Kubo S, Toyoda H, Nishina T, Ohba M, Hosokawa R, Kimura T, Tamaki N, et al. Cardiac functional analysis with multi-detector row CT and segmental reconstruction algorithm: comparison with echocardiography, SPECT, and MR imaging. *Radiology*, 234(2):381–90, 2005.

[97]   Rajappan K, Livieratos L, Camici PG, Pennell DJ. Measurement of ventricular volumes and function: a comparison of gated PET and cardiovascular magnetic resonance. *J Nucl Med*, 43(6):806–10, 2002.

[98]   Freiberg J, Hove JD, Kofoed KF, Fritz-Hansen T, Holm S, Larsson HB, Kelbaek H. Absolute quantitation of left ventricular wall and cavity parameters using ECG-gated PET. *J Nucl Cardiol*, 11(1):38–46, 2004.

[99]   Schaefer WM, Lipke CS, Nowak B, Kaiser HJ, Reinartz P, Buecker A, Krombach GA, Buell U, Kuhl HP. Validation of QGS and 4D-MSPECT for quantification of left ventricular volumes and ejection fraction from gated 18F-FDG PET: comparison with cardiac MRI. *J Nucl Med*, 45(1):74–9, 2004.

[100] Slart RH, Bax JJ, de Jong RM, de Boer J, Lamb HJ, Mook PH, Willemsen AT, Vaalburg W, van Veldhuisen DJ, Jager PL. Comparison of gated PET with MRI for evaluation of left ventricular function in patients with coronary artery disease. *J Nucl Med*, 45(2):176–82, 2004.

[101] Schaefer WM, Lipke CS, Nowak B, Kaiser HJ, Buecker A, Krombach GA, Buell U, Kuhl HP. Validation of an evaluation routine for left ventricular volumes, ejection fraction and wall motion from gated cardiac FDG PET: a comparison with cardiac magnetic resonance imaging. *Eur J Nucl Med Mol Imaging*, 30(4):545–53, 2003.

[102] Schlosser T, Pagonidis K, Herborn CU, Hunold P, Waltering KU, Lauenstein TC, Barkhausen J. Assessment of left ventricular parameters using 16-MDCT and new software for endocardial and epicardial border delineation. *AJR Am J Roentgenol*, 184(3):765–73, 2005.

[103] Mahnken AH, Koos R, Katoh M, Spuentrup E, Busch P, Wildberger JE, Kuhl HP, Gunther RW. Sixteen-slice spiral CT versus MR imaging for the assessment of left ventricular function in acute myocardial infarction. *Eur Radiol*, 15(4):714–20, 2005.

[104] Holman ER, Buller VG, de Roos A, van der Geest RJ, Baur LH, van der Laarse A, Bruschke AV, Reiber JH, van der Wall EE. Detection and quantification of dysfunctional myocardium by magnetic resonance imaging. A new three-dimensional method for quantitative wall-thickening analysis. *Circulation*, 95(4):924–31, 1997.

[105] van Rugge FP, van der Wall EE, Spanjersberg SJ, de Roos A, Matheijssen NA, Zwinderman AH, van Dijkman PR, Reiber JH, Bruschke AV. Magnetic resonance imaging during dobutamine stress for detection and localization of coronary artery disease. Quantitative wall motion analysis using a modification of the centerline method. *Circulation*, 90(1):127–38, 1994.

[106] Cain PA, Ugander M, Palmer J, Carlsson M, Heiberg E, Arheden H. Quantitative polar representation of left ventricular myocardial perfusion, function and viability using SPECT and cardiac magnetic resonance: initial results. *Clin Physiol Funct Imaging*, 25(4):215–22, 2005.

[107] Haendchen RV, Wyatt HL, Maurer G, Zwehl W, Bear M, Meerbaum S, Corday E. Quantitation of regional cardiac function by two-dimensional echocardiography. I. Patterns of contraction in the normal left ventricle. *Circulation*, 67(6):1234–45, 1983.

[108] Hatle L, Sutherland GR. Regional myocardial function–a new approach. *Eur Heart J*, 21(16):1337–57, 2000.

[109] Gibson DG, Prewitt TA, Brown DJ. Analysis of left ventricular wall movement during isovolumic relaxation and its relation to coronary artery disease. *Br Heart J*, 38(10):1010–9, 1976.

[110] Azhari H, Sideman S, Weiss JL, Shapiro EP, Weisfeldt ML, Graves WL, Rogers WJ, Beyar R. Three-dimensional mapping of acute ischemic regions using MRI: wall thickening versus motion analysis. *Am J Physiol*, 259(5 Pt 2):H1492–503, 1990.

[111] Sheehan FH, Bolson EL, Dodge HT, Mathey DG, Schofer J, Woo HW. Advantages and applications of the centerline method for characterizing regional ventricular function. *Circulation*, 74(2):293–305, 1986.

[112] Rademakers FE, Rogers WJ, Guier WH, Hutchins GM, Siu CO, Weisfeldt ML, Weiss JL, Shapiro EP. Relation of regional cross-fiber shortening to wall thickening in the intact heart. Three-dimensional strain analysis by NMR tagging. *Circulation*, 89(3):1174–82, 1994.

[113] Gotte MJ, van Rossum AC, Twisk JWR, Kuijer JPA, Marcus JT, Visser CA. Quantification of regional contractile function after infarction: strain analysis superior to wall thickening analysis in discriminating infarct from remote myocardium. *J Am Coll Cardiol*, 37(3):808–17, 2001.

[114] Heimdal A, Stoylen A, Torp H, Skjaerpe T. Real-time strain rate imaging of the left ventricle by ultrasound. *J Am Soc Echocardiogr*, 11(11):1013–9, 1998.

[115] Hachamovitch R, Berman DS. The use of nuclear cardiology in clinical decision making. *Semin Nucl Med*, 35(1):62–72, 2005.

[116] Hachamovitch R, Hayes SW, Friedman JD, Cohen I, Berman DS. Comparison of the short-term survival benefit associated with revascularization compared with medical therapy in patients with no prior coronary artery disease undergoing stress myocardial perfusion single photon emission computed tomography. *Circulation*, 107(23):2900–7, 2003.

[117] Gould KL, Schelbert HR, Phelps ME, Hoffman EJ. Noninvasive assessment of coronary stenoses with myocardial perfusion imaging during pharmacologic coronary vasodilatation. V. Detection of 47 percent diameter coronary stenosis with intravenous nitrogen-13 ammonia and emission-computed tomography in intact dogs. *Am J Cardiol*, 43(2):200–8, 1979.

[118] Schelbert HR, Wisenberg G, Phelps ME, Gould KL, Henze E, Hoffman EJ, Gomes A, Kuhl DE. Noninvasive assessment of coronary stenoses by myocardial imaging during pharmacologic coronary vasodilation. VI. Detection of coronary artery disease in human beings with intravenous N-13 ammonia and positron computed tomography. *Am J Cardiol*, 49(5):1197–207, 1982.

[119] Wei K, Jayaweera AR, Firoozan S, Linka A, Skyba DM, Kaul S. Quantification of myocardial blood flow with ultrasound-induced destruction of microbubbles administered as a constant venous infusion. *Circulation*, 97(5):473–83, 1998.

[120] Porter TR, Xie F, Silver M, Kricsfeld D, Oleary E. Real-time perfusion imaging with low mechanical index pulse inversion Doppler imaging. *J Am Coll Cardiol*, 37(3):748–53, 2001.

[121] Kaul S, Senior R, Dittrich H, Raval U, Khattar R, Lahiri A. Detection of coronary artery disease with myocardial contrast echocardiography: comparison with 99mTc-sestamibi single-photon emission computed tomography. *Circulation*, 96(3):785–92, 1997.

[122] Jucquois I, Nihoyannopoulos P, D'Hondt AM, Roelants V, Robert A, Melin JA, Glass D, Vanoverschelde JL. Comparison of myocardial contrast echocardiography with NC100100 and (99m)Tc sestamibi SPECT for detection of resting myocardial perfusion abnormalities in patients with previous myocardial infarction. *Heart*, 83(5):518–24, 2000.

[123] Schwitter J, Nanz D, Kneifel S, Bertschinger K, Buchi M, Knusel PR, Marincek B, Luscher TF, von Schulthess GK. Assessment of myocardial perfusion in coronary artery disease by magnetic resonance: a comparison with positron emission tomography and coronary angiography. *Circulation*, 103(18):2230–5, 2001.

[124] Lee DC, Simonetti OP, Harris KR, Holly TA, Judd RM, Wu E, Klocke FJ. Magnetic resonance versus radionuclide pharmacological stress perfusion imaging for flow-limiting stenoses of varying severity. *Circulation*, 110(1):58–65, 2004.

[125] Wolff SD, Schwitter J, Coulden R, Friedrich MG, Bluemke DA, Biederman RW, Martin ET, Lansky AJ, Kashanian F, et al. Myocardial first-pass perfusion magnetic resonance imaging: a multicenter dose-ranging study. *Circulation*, 110(6):732–7, 2004.

[126] Paetsch I, Jahnke C, Wahl A, Gebker R, Neuss M, Fleck E, Nagel E. Comparison of dobutamine stress magnetic resonance, adenosine stress magnetic resonance, and adenosine stress magnetic resonance perfusion. *Circulation*, 110(7):835–42, 2004.

[127] Ludman PF, Coats AJ, Burger P, Yang GZ, Poole-Wilson PA, Underwood SR, Rees RS. Validation of measurement of regional myocardial perfusion in humans by ultrafast x-ray computed tomography. *Am J Card Imaging*, 7(4):267–79, 1993.

[128] Nikolaou K, Sanz J, Poon M, Wintersperger BJ, Ohnesorge B, Rius T, Fayad ZA, Reiser MF, Becker CR. Assessment of myocardial perfusion and viability from routine contrast-enhanced 16-detector-row computed tomography of the heart: preliminary results. *Eur Radiol*, 15(5):864–71, 2005.

[129] Bax JJ, van der Wall EE, de Roos A. In BL Zaret, GA Beller, editors, *Clinical nuclear cardiology. State of the art and future directions.*, pages 535–55. Mosby, Philadelphia, 2005.

[130] Nagel E, Lehmkuhl HB, Bocksch W, Klein C, Vogel U, Frantz E, Ellmer A, Dreysse S, Fleck E. Noninvasive diagnosis of ischemia-induced wall motion abnormalities with the use of high-dose dobutamine stress MRI: comparison with dobutamine stress echocardiography. *Circulation*, 99(6):763–70, 1999.

[131] Nagel E, Lehmkuhl HB, Klein C, Schneider U, Frantz E, Ellmer A, Bocksch W, Dreysse S, Fleck E. [Influence of image quality on the diagnostic accuracy of dobutamine stress magnetic resonance imaging in comparison with dobutamine stress echocardiography for the noninvasive detection of myocardial ischemia]. *Z Kardiol*, 88(9):622–30, 1999.

[132] DePuey EG, Rozanski A. Using gated technetium-99m-sestamibi SPECT to characterize fixed myocardial defects as infarct or artifact. *J Nucl Med*, 36(6):952–5, 1995.

[133] Smanio PE, Watson DD, Segalla DL, Vinson EL, Smith WH, Beller GA. Value of gating of technetium-99m sestamibi single-photon emission computed tomographic imaging. *J Am Coll Cardiol*, 30(7):1687–92, 1997.

[134] Shaw LJ, Iskandrian AE. Prognostic value of gated myocardial perfusion SPECT. *J Nucl Cardiol*, 11(2):171–85, 2004.

[135] Johnson KR, Patel SJ, Whigham A, Hakim A, Pettigrew RI, Oshinski JN. Three-dimensional, time-resolved motion of the coronary arteries. *J Cardiovasc Magn Reson*, 6(3):663–73, 2004.

[136] Leschka S, Alkadhi H, Plass A, Desbiolles L, Grunenfelder J, Marincek B, Wildermuth S. Accuracy of MSCT coronary angiography with 64-slice technology: first experience. *Eur Heart J*, 26(15):1482–7, 2005.

[137] Shaw LJ, Raggi P, Schisterman E, Berman DS, Callister TQ. Prognostic value of cardiac risk factors and coronary artery calcium screening for all-cause mortality. *Radiology*, 228(3):826–33, 2003.

[138] Berman DS, Wong ND, Gransar H, Miranda-Peats R, Dahlbeck J, Hayes SW, Friedman JD, Kang X, Polk D, et al. Relationship between stress-induced myocardial ischemia and atherosclerosis measured by coronary calcium tomography. *J Am Coll Cardiol*, 44(4):923–30, 2004.

[139] Schuijf JD, Bax JJ, Shaw LJ. Meta-analysis of comparative diagnostic performance of magnetic resonance imaging and multi-sclice computed tomography for non-invasive coronary angiography. *Am Heart J*, 2005 (in press).

[140] Bax JJ, Poldermans D, Elhendy A, Boersma E, Rahimtoola SH. Sensitivity, specificity, and predictive accuracies of various noninvasive techniques for detecting hibernating myocardium. *Curr Probl Cardiol*, 26(2):141–86, 2001.

[141] Bax JJ, van der Wall EE, Harbinson M. Radionuclide techniques for the assessment of myocardial viability and hibernation. *Heart*, 90 Suppl 5:v26–33, 2004.

[142] Bax JJ. FDG imaging should be considered the preferred technique for accurate assessment of myocardial viability. *Eur J Nucl Med Mol Imaging*, 32(7):829–31, 2005.

[143] Tillisch J, Brunken R, Marshall R, Schwaiger M, Mandelkern M, Phelps M, Schelbert H. Reversibility of cardiac wall-motion abnormalities predicted by positron tomography. *N Engl J Med*, 314(14):884–8, 1986.

[144] Bax JJ, Patton JA, Poldermans D, Elhendy A, Sandler MP. 18-Fluorodeoxyglucose imaging with positron emission tomography and single photon emission computed tomography: cardiac applications. *Semin Nucl Med*, 30(4):281–98, 2000.

[145] Beanlands RS, Hendry PJ, Masters RG, deKemp RA, Woodend K, Ruddy TD. Delay in revascularization is associated with increased mortality rate in patients with severe left ventricular dysfunction and viable myocardium on fluorine 18-fluorodeoxyglucose positron emission tomography imaging. *Circulation*, 98(19 Suppl):II51–6, 1998.

[146] Beanlands RS, deKemp RA, Smith S, Johansen H, Ruddy TD. F-18-fluorodeoxyglucose PET imaging alters clinical decision making in patients with impaired ventricular function. *Am J Cardiol*, 79(8):1092–5, 1997.

[147] Bax JJ, Poldermans D, Elhendy A, Cornel JH, Boersma E, Rambaldi R, Roelandt JR, Fioretti PM. Improvement of left ventricular ejection fraction, heart failure symptoms and prognosis after revascularization in patients with chronic coronary artery disease and viable myocardium detected by dobutamine stress echocardiography. *J Am Coll Cardiol*, 34(1):163–9, 1999.

[148] Shimoni S, Frangogiannis NG, Aggeli CJ, Shan K, Quinones MA, Espada R, Letsou GV, Lawrie GM, Winters WL, et al. Microvascular structural correlates of myocardial contrast echocardiography in patients with coronary artery disease and left ventricular dysfunction: implications for the assessment of myocardial hibernation. *Circulation*, 106(8):950–6, 2002.

[149] Korosoglou G, Hansen A, Hoffend J, Gavrilovic G, Wolf D, Zehelein J, Haberkorn U, Kuecherer H. Comparison of real-time myocardial contrast echocardiography for the assessment of myocardial viability with fluorodeoxyglucose-18 positron emission tomography and dobutamine stress echocardiography. *Am J Cardiol*, 94(5):570–6, 2004.

[150] Levine MG, McGill CC, Ahlberg AW, White MP, Giri S, Shareef B, Waters D, Heller GV. Functional assessment with electrocardiographic gated single-photon emission computed tomography improves the ability of technetium-99m sestamibi myocardial perfusion imaging to predict myocardial viability in patients undergoing revascularization. *Am J Cardiol*, 83(1):1–5, 1999.

[151] Leoncini M, Marcucci G, Sciagra R, Mondanelli D, Traini AM, Magni M, Frascarelli F, Mennuti A, Dabizzi RP. Comparison of baseline and low-dose dobutamine technetium-99m sestamibi scintigraphy with low-dose dobutamine echocardiography for predicting functional recovery after revascularization. *Am J Cardiol*, 86(2):153–7, 2000.

[152] Baer FM, Voth E, Schneider CA, Theissen P, Schicha H, Sechtem U. Comparison of low-dose dobutamine-gradient-echo magnetic resonance imaging and positron emission tomography with [18F]fluorodeoxyglucose in patients with chronic coronary artery disease. A functional and morphological approach to the detection of residual myocardial viability. *Circulation*, 91(4):1006–15, 1995.

[153] Baer FM, Theissen P, Schneider CA, Voth E, Sechtem U, Schicha H, Erdmann E. Dobutamine magnetic resonance imaging predicts contractile recovery of chronically dysfunctional myocardium after successful revascularization. *J Am Coll Cardiol*, 31(5):1040–8, 1998.

[154] Sayad DE, Willett DL, Hundley WG, Grayburn PA, Peshock RM. Dobutamine magnetic resonance imaging with myocardial tagging quantitatively predicts improvement in regional function after revascularization. *Am J Cardiol*, 82(9):1149–51, A10, 1998.

[155] Shan K, Constantine G, Sivananthan M, Flamm SD. Role of cardiac magnetic resonance imaging in the assessment of myocardial viability. *Circulation*, 109(11):1328–34, 2004.

[156] Kim RJ, Fieno DS, Parrish TB, Harris K, Chen EL, Simonetti O, Bundy J, Finn JP, Klocke FJ, Judd RM. Relationship of MRI delayed contrast enhancement to irreversible injury, infarct age, and contractile function. *Circulation*, 100(19):1992–2002., 1999.

[157] Fieno DS, Kim RJ, Chen EL, Lomasney JW, Klocke FJ, Judd RM. Contrast-enhanced magnetic resonance imaging of myocardium at risk: distinction between reversible and irreversible injury throughout infarct healing. *J Am Coll Cardiol*, 36(6):1985–91, 2000.

[158] Rehwald WG, Fieno DS, Chen EL, Kim RJ, Judd RM. Myocardial magnetic resonance imaging contrast agent concentrations after reversible and irreversible ischemic injury. *Circulation*, 105(2):224–9, 2002.

[159] Choi KM, Kim RJ, Gubernikoff G, Vargas JD, Parker M, Judd RM. Transmural extent of acute myocardial infarction predicts long-term improvement in contractile function. *Circulation*, 104(10):1101–7, 2001.

[160] Beek AM, Kuhl HP, Bondarenko O, Twisk JW, Hofman MB, van Dockum WG, Visser CA, van Rossum AC. Delayed contrast-enhanced magnetic resonance imaging for the prediction of regional functional improvement after acute myocardial infarction. *J Am Coll Cardiol*, 42(5):895–901, 2003.

[161] Kim RJ, Wu E, Rafael A, Chen EL, Parker MA, Simonetti O, Klocke FJ, Bonow RO, Judd RM. The use of contrast-enhanced magnetic resonance imaging to identify reversible myocardial dysfunction. *N Engl J Med*, 343(20):1445–53, 2000.

[162] Knuesel PR, Nanz D, Wyss C, Buechi M, Kaufmann PA, von Schulthess GK, Luscher TF, Schwitter J. Characterization of dysfunctional myocardium by positron emission tomography and magnetic resonance: relation to functional outcome after revascularization. *Circulation*, 108(9):1095–100, 2003.

[163] Selvanayagam JB, Kardos A, Francis JM, Wiesmann F, Petersen SE, Taggart DP, Neubauer S. Value of delayed-enhancement cardiovascular magnetic resonance imaging in predicting myocardial viability after surgical revascularization. *Circulation*, 110(12):1535–41, 2004.

[164] Schvartzman PR, Srichai MB, Grimm RA, Obuchowski NA, Hammer DF, McCarthy PM, Kasper JM, White RD. Nonstress delayed-enhancement magnetic resonance imaging of the myocardium predicts improvement of function after revascularization for chronic ischemic heart disease with left ventricular dysfunction. *Am Heart J*, 146(3):535–41, 2003.

[165] Bello D, Shah DJ, Farah GM, Di Luzio S, Parker M, Johnson MR, Cotts WG, Klocke FJ, Bonow RO, et al. Gadolinium cardiovascular magnetic resonance predicts reversible myocardial dysfunction and remodeling in patients with heart failure undergoing beta-blocker therapy. *Circulation*, 108(16):1945–53, 2003.

[166] Mahrholdt H, Wagner A, Holly TA, Elliott MD, Bonow RO, Kim RJ, Judd RM. Reproducibility of chronic infarct size measurement by contrast-enhanced magnetic resonance imaging. *Circulation*, 106(18):2322–7, 2002.

[167] Klein C, Nekolla SG, Bengel FM, Momose M, Sammer A, Haas F, Schnackenburg B, Delius W, Mudra H, et al. Assessment of myocardial viability with contrast-enhanced magnetic resonance imaging: comparison with positron emission tomography. *Circulation*, 105(2):162–7, 2002.

[168] Kuhl HP, Beek AM, van der Weerdt AP, Hofman MB, Visser CA, Lammertsma AA, Heussen N, Visser FC, van Rossum AC. Myocardial viability in chronic ischemic heart disease: comparison of contrast-enhanced magnetic resonance imaging with (18)F-fluorodeoxyglucose positron emission tomography. *J Am Coll Cardiol*, 41(8):1341–8, 2003.

[169] Wagner A, Mahrholdt H, Holly TA, Elliott MD, Regenfus M, Parker M, Klocke FJ, Bonow RO, Kim RJ, Judd RM. Contrast-enhanced MRI and routine single photon emission computed tomography (SPECT) perfusion imaging for detection of subendocardial myocardial infarcts: an imaging study. *Lancet*, 361(9355):374–9, 2003.

[170] Hedstrom E, Palmer J, Ugander M, Arheden H. Myocardial SPECT perfusion defect size compared to infarct size by delayed gadolinium-enhanced magnetic resonance imaging in patients with acute or chronic infarction. *Clin Physiol Funct Imaging*, 24(6):380–6, 2004.

[171] Slomka PJ, Fieno D, Thomson L, Friedman JD, Hayes SW, Germano G, Berman DS. Automatic detection and size quantification of infarcts by myocardial perfusion SPECT: clinical validation by delayed-enhancement MRI. *J Nucl Med*, 46(5):728–35, 2005.

[172] Janardhanan R, Moon JC, Pennell DJ, Senior R. Myocardial contrast echocardiography accurately reflects transmurality of myocardial necrosis and predicts contractile reserve after acute myocardial infarction. *Am Heart J*, 149(2):355–62, 2005.

[173] McCrohon JA, Lyne JC, Rahman SL, Lorenz CH, Underwood SR, Pennell DJ. Adjunctive role of cardiovascular magnetic resonance in the assessment of patients with inferior attenuation on myocardial perfusion SPECT. *J Cardiovasc Magn Reson*, 7(2):377–82, 2005.

[174] Ricciardi MJ, Wu E, Davidson CJ, Choi KM, Klocke FJ, Bonow RO, Judd RM, Kim RJ. Visualization of discrete microinfarction after percutaneous coronary intervention associated with mild creatine kinase-MB elevation. *Circulation*, 103(23):2780–3, 2001.

[175] Steuer J, Bjerner T, Duvernoy O, Jideus L, Johansson L, Ahlstrom H, Stahle E, Lindahl B. Visualisation and quantification of peri-operative myocardial infarction after coronary artery bypass surgery with contrast-enhanced magnetic resonance imaging. *Eur Heart J*, 25(15):1293–9, 2004.

[176] Van Hoe L, Vanderheyden M. Ischemic cardiomyopathy: value of different MRI techniques for prediction of functional recovery after revascularization. *AJR Am J Roentgenol*, 182(1):95–100, 2004.

[177] Gutberlet M, Frohlich M, Mehl S, Amthauer H, Hausmann H, Meyer R, Siniawski H, Ruf J, Plotkin M, et al. Myocardial viability assessment in patients with highly impaired left ventricular function: comparison of delayed enhancement, dobutamine stress MRI, end-diastolic wall thickness, and TI201-SPECT with functional recovery after revascularization. *Eur Radiol*, 15(5):872–80, 2005.

[178] Wellnhofer E, Olariu A, Klein C, Grafe M, Wahl A, Fleck E, Nagel E. Magnetic resonance low-dose dobutamine test is superior to SCAR quantification for the prediction of functional recovery. *Circulation*, 109(18):2172–4, 2004.

[179] Kaandorp TA, Bax JJ, Schuijf JD, Viergever EP, van Der Wall EE, de Roos A, Lamb HJ. Head-to-head comparison between contrast-enhanced magnetic resonance imaging and dobutamine magnetic resonance imaging in men with ischemic cardiomyopathy. *Am J Cardiol*, 93(12):1461–4, 2004.

[180] Kim RJ, Manning WJ. Viability assessment by delayed enhancement cardiovascular magnetic resonance: will low-dose dobutamine dull the shine? *Circulation*, 109(21):2476–9, 2004.

[181] Higgins CB, Siemers PT, Newell JD, Schmidt W. Role of iodinated contrast material in the evaluation of myocardial infarction by computerized transmission tomography. *Invest Radiol*, 15(6 Suppl):S176–82, 1980.

[182] Mahnken AH, Koos R, Katoh M, Wildberger JE, Spuentrup E, Buecker A, Gunther RW, Kuhl HP. Assessment of myocardial viability in reperfused acute myocardial infarction using 16-slice computed tomography in comparison to magnetic resonance imaging. *J Am Coll Cardiol*, 45(12):2042–7, 2005.

[183] Bonow RO. Myocardial viability and prognosis in patients with ischemic left ventricular dysfunction. *J Am Coll Cardiol*, 39(7):1159–62, 2002.

[184] Mahrholdt H, Wagner A, Judd RM, Sechtem U, Kim RJ. Delayed enhancement cardiovascular magnetic resonance assessment of non-ischaemic cardiomyopathies. *Eur Heart J*, 2005.

[185] Pennell DJ. Ventricular volume and mass by CMR. *J Cardiovasc Magn Reson*, 4(4):507–13, 2002.

[186] Chan J, Wahi S, Cain P, Marwick TH. Anatomical M-mode: A novel technique for the quantitative evaluation of regional wall motion analysis during dobutamine echocardiography. *Int J Card Imaging*, 16(4):247–55, 2000.

[187] Fujita N, Chazouilleres AF, Hartiala JJ, O'Sullivan M, Heidenreich P, Kaplan JD, Sakuma H, Foster E, Caputo GR, Higgins CB. Quantification of mitral regurgitation by velocity-encoded cine nuclear magnetic resonance imaging. *J Am Coll Cardiol*, 23(4):951–8, 1994.

[188] Sechtem U, Pflugfelder PW, Cassidy MM, White RD, Cheitlin MD, Schiller NB, Higgins CB. Mitral or aortic regurgitation: quantification of regurgitant volumes with cine MR imaging. *Radiology*, 167(2):425–30, 1988.

[189] Tong CY, Prato FS, Wisenberg G, Lee TY, Carroll E, Sandler D, Wills J, Drost D. Measurement of the extraction efficiency and distribution volume for Gd-DTPA in normal and diseased canine myocardium. *Magn Reson Med*, 30(3):337–46, 1993.

[190] Flacke SJ, Fischer SE, Lorenz CH. Measurement of the gadopentetate dimeglumine partition coefficient in human myocardium in vivo: normal distribution and elevation in acute and chronic infarction. *Radiology*, 218(3):703–10, 2001.

[191] Altman DG. *Practical Statistics for Medical Research*. Chapman & Hall, London, 1991.

[192] Borges-Neto S, Shaw LK. The added value of simultaneous myocardial perfusion and left ventricular function. *Curr Opin Cardiol*, 14(6):460–3, 1999.

[193] Marwick TH, Shaw LJ, Lauer MS, Kesler K, Hachamovitch R, Heller GV, Travin MI, Borges-Neto S, Berman DS, Miller DD. The noninvasive prediction of cardiac mortality in men and women with known or suspected coronary artery disease. Economics of Noninvasive Diagnosis (END) Study Group. *Am J Med*, 106(2):172–8, 1999.

[194] Ginzton LE, Conant R, Brizendine M, Thigpen T, Laks MM. Quantitative analysis of segmental wall motion during maximal upright dynamic exercise: variability in normal adults. *Circulation*, 73(2):268–75, 1986.

[195] Aletras AH, Wen H. Mixed echo train acquisition displacement encoding with stimulated echoes: an optimized DENSE method for in vivo functional imaging of the human heart. *Magn Reson Med*, 46(3):523–34, 2001.

[196] Weiss JL, Bulkley BH, Hutchins GM, Mason SJ. Two-dimensional echocardiographic recognition of myocardial injury in man: comparison with postmortem studies. *Circulation*, 63(2):401–8, 1981.

[197] Lieberman AN, Weiss JL, Jugdutt BI, Becker LC, Bulkley BH, Garrison JG, Hutchins GM, Kallman CA, Weisfeldt ML. Two-dimensional echocardiography and infarct size: relationship of regional wall motion and thickening to the extent of myocardial infarction in the dog. *Circulation*, 63(4):739–46, 1981.

[198] Ellis SG, Henschke CI, Sandor T, Wynne J, Kloner RA. Relation between the transmural extent of acute myocardial infarction and associated myocardial contractility two weeks after infarction. *Am J Cardiol*, 55(11):1412–6, 1985.

[199] Mahrholdt H, Wagner A, Parker M, Regenfus M, Fieno DS, Bonow RO, Kim RJ, Judd RM. Relationship of contractile function to transmural extent of infarction in patients with chronic coronary artery disease. *J Am Coll Cardiol*, 42(3):505–12, 2003.

[200] Ingkanisorn WP, Rhoads KL, Aletras AH, Kellman P, Arai AE. Gadolinium delayed enhancement cardiovascular magnetic resonance correlates with clinical measures of myocardial infarction. *J Am Coll Cardiol*, 43(12):2253–9, 2004.

[201] Kolipaka A, Chatzimavroudis GP, White RD, Lieber ML, Setser RM. Relationship between the extent of non-viable myocardium and regional left ventricular function in chronic ischemic heart disease. *J Cardiovasc Magn Reson*, 7(3):573–9, 2005.

[202] Palmeri ST, Harrison DG, Cobb FR, Morris KG, Harrell FE, Ideker RE, Selvester RH, Wagner GS. A QRS scoring system for assessing left ventricular function after myocardial infarction. *N Engl J Med*, 306(1):4–9, 1982.

[203] Christian TF, Behrenbeck T, Pellikka PA, Huber KC, Chesebro JH, Gibbons RJ. Mismatch of left ventricular function and infarct size demonstrated by technetium-99m isonitrile imaging after reperfusion therapy for acute myocardial infarction: identification of myocardial stunning and hyperkinesia. *J Am Coll Cardiol*, 16(7):1632–8, 1990.

[204] Christian TF, Behrenbeck T, Gersh BJ, Gibbons RJ. Relation of left ventricular volume and function over one year after acute myocardial infarction to infarct size determined by technetium-99m sestamibi. *Am J Cardiol*, 68(1):21–6, 1991.

[205] Sciagra R, Imperiale A, Antoniucci D, Migliorini A, Parodi G, Comis G, Pupi A. Relationship of infarct size and severity versus left ventricular ejection fraction and volumes obtained from 99mTc-sestamibi gated single-photon emission computed tomography in patients treated with primary percutaneous coronary intervention. *Eur J Nucl Med Mol Imaging*, 31(7):969–74, 2004.

[206] Burns RJ, Gibbons RJ, Yi Q, Roberts RS, Miller TD, Schaer GL, Anderson JL, Yusuf S. The relationships of left ventricular ejection fraction, end-systolic volume index and infarct size to six-month mortality after hospital discharge following myocardial infarction treated by thrombolysis. *J Am Coll Cardiol*, 39(1):30–6, 2002.

[207] Topol EJ, Weiss JL, Guzman PA, Dorsey-Lima S, Blanck TJ, Humphrey LS, Baumgartner WA, Flaherty JT, Reitz BA. Immediate improvement of dysfunctional myocardial segments after coronary revascularization: detection by intraoperative transesophageal echocardiography. *J Am Coll Cardiol*, 4(6):1123–34, 1984.

[208] Elsasser A, Schlepper M, Klovekorn WP, Cai WJ, Zimmermann R, Muller KD, Strasser R, Kostin S, Gagel C, et al. Hibernating myocardium: an incomplete adaptation to ischemia. *Circulation*, 96(9):2920–31, 1997.

[209] Haas F, Augustin N, Holper K, Wottke M, Haehnel C, Nekolla S, Meisner H, Lange R, Schwaiger M. Time course and extent of improvement of dysfunctioning myocardium in patients with coronary artery disease and severely depressed left ventricular function after revascularization: correlation with positron emission tomographic findings. *J Am Coll Cardiol*, 36(6):1927–34, 2000.

[210] Haas F, Jennen L, Heinzmann U, Augustin N, Wottke M, Schwaiger M, Lange R. Ischemically compromised myocardium displays different time-courses of functional recovery: correlation with morphological alterations? *Eur J Cardiothorac Surg*, 20(2):290–8, 2001.

[211] Bax JJ, Visser FC, Poldermans D, Elhendy A, Cornel JH, Boersma E, van Lingen A, Fioretti PM, Visser CA. Time course of functional recovery of stunned and hibernating segments after surgical revascularization. *Circulation*, 104(12 Suppl 1):I314–8, 2001.

[212] Maes A, Flameng W, Nuyts J, Borgers M, Shivalkar B, Ausma J, Bormans G, Schiepers C, De Roo M, Mortelmans L. Histological alterations in chronically hypoperfused myocardium. Correlation with PET findings. *Circulation*, 90(2):735–45, 1994.

[213] Maes AF, Borgers M, Flameng W, Nuyts JL, van de Werf F, Ausma JJ, Sergeant P, Mortelmans LA. Assessment of myocardial viability in chronic coronary artery disease using technetium-99m sestamibi SPECT. Correlation with histologic and positron emission tomographic studies and functional follow-up. *J Am Coll Cardiol*, 29(1):62–8, 1997.

[214] Kaprielian RR, Gunning M, Dupont E, Sheppard MN, Rothery SM, Underwood R, Pennell DJ, Fox K, Pepper J, et al. Downregulation of immunodetectable connexin43 and decreased gap junction size in the pathogenesis of chronic hibernation in the human left ventricle. *Circulation*, 97(7):651–60, 1998.